Published for SISSA by Springer

Received: May 15, 2025
Revised: October 13, 2025
Accepted: November 24, 2025
Published: January 9, 2026

NNLO predictions with nonlocal subtractions and fiducial power corrections in GENEVA

Simone Alioli,[a] **Georgios Billis**,[a,b] **Alessandro Broggio**[c] **and Giovanni Stagnitto**[a]

[a] *Università degli Studi di Milano-Bicocca & INFN Sezione di Milano-Bicocca, Piazza della Scienza 3, Milano 20126, Italy*
[b] *Paul Scherrer Institut, CH-5232 Villigen PSI, Switzerland*
[c] *Faculty of Physics, University of Vienna, Boltzmanngasse 5, A-1090 Wien, Austria*

E-mail: simone.alioli@unimib.it, georgios.billis@psi.ch, alessandro.broggio@univie.ac.at, giovanni.stagnitto@edu.unige.it

Abstract: We present the implementation of next-to-next-to-leading order (NNLO) QCD fully-differential corrections within the Geneva framework, for both colour-singlet and colour-singlet+jet processes at hadron colliders, by employing a nonlocal subtraction approach. In particular, we discuss the implementation details and the challenges that arise when utilizing a dynamical infrared cutoff parameter. Additionally, we combine the subtraction with the projection-to-Born method in order to include fiducial power corrections. As a test case, we provide predictions for Drell-Yan and Z+jet production at the LHC, using N-jettiness as resolution variable. We validate the NNLO corrections of Geneva against nnlojet finding excellent agreement. Finally, we discuss how to extend our method to calculate the N^{3}LO QCD fully-differential corrections to colour-singlet production at hadron colliders.

Keywords: Higher-Order Perturbative Calculations, Effective Field Theories of QCD, Resummation, Specific QCD Phenomenology

ArXiv ePrint: 2504.11357

Open Access, © The Authors.
Article funded by SCOAP^3.

https://doi.org/10.1007/JHEP01(2026)065

JHEP01(2026)065

Contents

1 Introduction

The High Luminosity Large Hadron Collider (HL-LHC) is set to begin operations by the end of the decade, and will provide the LHC experiments with significantly larger data samples, up to an order of magnitude greater than the current baseline program. This will present a unique opportunity to achieve unprecedentedly precise measurements across the entire phase space, while also expanding the potential to detect deviations from Standard Model (SM) predictions across a wide range of processes and observables. In particular, the increased statistics will allow for highly accurate measurements of the high-energy tails of distributions, which are especially sensitive to new physics effects.

In order to ensure that the theoretical predictions match the precision of the experimental measurements at the LHC, it is essential to achieve at least next-to-next-to-leading order (NNLO) accuracy in the perturbative expansion in the strong coupling α_s when evaluating partonic cross sections of crucial benchmark processes, such as the production of electroweak bosons $(W^{\pm}, Z)$ [1–5].

Production processes of SM bosons in association with a hadronic jet are among the most frequently occurring reactions at hadron colliders and retain a large event rate. At they same time, they also offer the possibility to study more precisely the transverse momentum (q_T) spectrum of SM bosons, which is primarily caused by the recoil against emitted partons and depends on QCD dynamics. In particular, the production of a Z boson in association with a jet is a key process in probing SM physics, for example in fitting Parton Distribution Functions

JHEP01(2026)065

(PDFs) and measuring the strong coupling constant α_s [6, 7]. Furthermore, when the Z boson decays into invisible neutrinos, it is an important background for searches of physics beyond the SM that involve missing energy. Similarly, the Higgs+jet process allows for searches of non-standard Higgs couplings while the W+jet process serves as a background for dark matter searches [8, 9]. Precise predictions of the W-boson's transverse momentum are also crucial for accurate W-boson mass determinations [10–14]. In addition, NNLO predictions for colour-singlet+jet processes are fundamental ingredients for fully-differential calculations of Z/Higgs/W production at next-to-next-to-next-to-leading order (N^{3}LO) accuracy [15–24].

The evaluation of fully differential NNLO corrections requires the implementation of a subtraction or a slicing method to remove the infrared (IR) divergences that appear at intermediate stages of the calculation. In the last decade, NNLO predictions for processes with final-state jets at the LHC were obtained by different groups using local subtraction methods [25] such as the antenna subtraction scheme [26], the STRIPPER scheme [27, 28] as well as N-jettiness ($\mathcal{T}_N$) slicing [20, 29].

Nonlocal subtraction methods at NNLO which utilize as slicing variable either the transverse momentum (q_T) of the colour-singlet system [30–32] or of the hardest jet [33], or N-jettiness [29, 34–37] or a process-specific slicing parameter [38, 39], can be further refined in the presence of fiducial cuts by the inclusion of recoil effects [40, 41] or by the combination with the Projection-to-Born (P2B) method [42], as shown for the first time in ref. [43] and implemented up to NNLO in ref. [44]. This improvement allows to include fiducial power corrections (FPCs) below the IR cutoff parameter $\mathcal{T}_\delta$ for the observables that are sensitive to that. The inclusion of these effects allows to obtain a better agreement with local subtraction methods.

In this paper we present a novel implementation of nonlocal subtractions in combination with the P2B method for colour-singlet and colour-singlet+jet processes at the LHC. At variance with previous implementations which rely on a pure slicing approach, here we implemented a genuine nonlocal subtraction term which is integrated together with the NLO differential cross section for a resolved emission above $\mathcal{T}_\delta$. To the best of our knowledge, this is the first implementation of a genuinely nonlocal subtraction. This requires the introduction of normalized splitting functions that renders the subtraction terms differential in the higher multiplicity phase space of the resolved emission while preserving its dependence on the resolution variable. The primary challenge of this approach, when using a dynamic $\mathcal{T}_\delta$ parameter, lies in the need for a mapping of the splitting functions that preserves the variables which define the dynamical cutoff.

While the formulas that we derive are independent of specific resolution variables and can be applied to any suitable variable that correctly captures the IR regions of QCD in the limit where this variable approaches zero, in this work we present, as an example, results for the Z and Z+jet production processes by employing N-jettiness subtractions [34] in combination with the P2B method. Our implementation of nonlocal N-jettiness subtractions relies on the fixed order expansion up to relative $\mathcal{O}(\alpha_s^2)$ of leading power N^{3}LL resummation formulas for zero-jettiness ($\mathcal{T}_0$) [45, 46] and 1-jettiness ($\mathcal{T}_1$) [47], both defined in the frame where the colour-singlet system has zero rapidity. In the 0-jettiness case, we also supplement the leading power approximation with the leading next-to-leading power (NLP) logarithms which

JHEP01(2026)065

were computed in [48] and provide an improvement in the numerical efficiency and stability of subtractions, which allows for a larger $\mathcal{T}_\delta$ parameter. Unfortunately the corresponding leading-logarithm NLP contributions are not yet known for 1-jettiness. We also point out that for the Z+jet calculation we employ the 1-jettiness definition derived in ref. [47], which is based on an exclusive clustering procedure. This means that we recursively cluster together emissions using the $\mathcal{T}_1$ metric until we are left with one jet (see discussion in ref. [47]) and we don't rely on external jet clustering algorithms. We stress that this definition is different from the one used in refs. [29, 35, 49, 50], where the jet axis is determined a priori by employing an inclusive jet clustering procedure.

The results of this paper, besides providing independent NNLO calculations, are also crucial for the development of the GENEVA Monte Carlo (MC) event generator [45, 51–57]. Indeed they eliminate the potential need for a reweighting procedure, typically carried out with an external NNLO-accurate program, by directly providing instead the NNLO predictions for the N-jet cross section.

The manuscript is organized as follows. In section 2 we introduce the formulas which combine a nonlocal subtraction scheme with the P2B method in order to capture the fiducial power corrections. This formalism is general and can be applied to any suitable jet resolution variable and processes with any number of final-state jets. In section 3 we derive the relevant cross section formulas for generic N-jettiness variables in a form that is suitable for the implementation in the GENEVA framework. In section 4 we specify the subtraction formulas for colour-singlet and colour-singlet+jet processes and provide numerical results for Z and Z+jet using N-jettiness subtractions in combination with the P2B method, comparing our results to NNLOJET [26, 58–83]. In section 5 we discuss the extension of our approach to obtain N^{3}LO fully-differential predictions. We finally draw our conclusions in section 6.

2 Theoretical framework

We calculate the NNLO QCD corrections (δNNLO) to a generic observable $\mathcal{O}$, where the subtraction terms and their integrated counterparts are understood and not written out explicitly. For ease of notation we also omit flavour indices in the cross sections, which are implicitly given relative to a partonic channel. Summing over all relevant partonic channels we get the total NNLO corrections δNNLO, and adding it to the corresponding NLO results we obtain the total NNLO cross sections and distributions. Since the calculation of NLO corrections for a generic observable are easily obtained with fully-local subtraction methods, we will not discuss them further in this paper.

Our starting formula for the NNLO corrections is

$$\begin{aligned}\mathcal{O}_{\delta\mathrm{NNLO}}(\Phi_N) &= W(\Phi_N)\mathcal{O}(\Phi_N) + \int \frac{\mathrm{d}\Phi_{N+1}}{\mathrm{d}\Phi_N} RV(\Phi_{N+1})\mathcal{O}(\Phi_{N+1}) \\ &\quad + \int \frac{\mathrm{d}\Phi_{N+2}}{\mathrm{d}\Phi_N} RR(\Phi_{N+2})\mathcal{O}(\Phi_{N+2}) \\ &\equiv \frac{\mathrm{d}\sigma_N^{\delta\mathrm{NNLO}}}{\mathrm{d}\Phi_N}\mathcal{O}(\Phi_{N+X})\,,\end{aligned} \tag{2.1}$$

JHEP01(2026)065

where in the last line we have defined the NNLO correction cross section at fixed underlying-Born[1] kinematics $\mathrm{d}\sigma_N^{\delta\mathrm{NNLO}}/\mathrm{d}\Phi_N$ and the notation $\mathcal{O}(\Phi_{N+X})$ indicates that the observable is evaluated at the exact kinematic configuration for each one of the NNLO contributions: double virtual $W(\Phi_N)$, real-virtual $RV(\Phi_{N+1})$ and double real $RR(\Phi_{N+2})$.

The formula above implies that for processes which are already divergent at the Born level, a set of process-defining cuts must be applied to all contributions. A typical example in the process $pp \to Z$+jet would be a cut on the transverse momentum (q_T) of the Z-boson or on zero-jettiness ($\mathcal{T}_0$).

One can now add and subtract the observable evaluated on the projected Born phase space $\mathcal{O}(\Phi_N)$ and obtain the equivalent formula

$$\mathcal{O}_{\delta\mathrm{NNLO}}(\Phi_N) = \frac{\mathrm{d}\sigma_N^{\delta\mathrm{NNLO}}}{\mathrm{d}\Phi_N}\mathcal{O}(\Phi_N) + \frac{\mathrm{d}\sigma_N^{\delta\mathrm{NNLO}}}{\mathrm{d}\Phi_N}\Big[\mathcal{O}(\Phi_{N+X}) - \mathcal{O}(\Phi_N)\Big]\,. \tag{2.2}$$

At this point, we observe that the double virtual term never contributes to the second addend of eq. (2.2), since its contribution is multiplied by the difference between the observable evaluated on the same Φ_N configuration, which is zero. Therefore, without doing any approximation, the second addend is exactly replaced by the cross section of the NLO corrections for the process with one extra parton, integrated over the additional radiation phase space at fixed the underlying-Born kinematics, i.e.

$$\mathcal{O}_{\delta\mathrm{NNLO}}(\Phi_N) = \frac{\mathrm{d}\sigma_N^{\delta\mathrm{NNLO}}}{\mathrm{d}\Phi_N}\mathcal{O}(\Phi_N) + \int\frac{\mathrm{d}\Phi_{N+1}}{\mathrm{d}\Phi_N}\frac{\mathrm{d}\sigma_{N+1}^{\delta\mathrm{NLO}}}{\mathrm{d}\Phi_{N+1}}\Big[\mathcal{O}(\Phi_{N+X}) - \mathcal{O}(\Phi_N)\Big]\,. \tag{2.3}$$

Eq. (2.3) is the essence of the projection-to-Born (P2B) method. In order to be practically applied, however, it still requires the knowledge of the exact NNLO corrections evaluated on the underlying-Born kinematics (first addend of eq. (2.3)). In the following we will show how this requirement can be circumvented by leveraging on a subtraction approach, which relies on an approximation of this term, that can be systematically improved until the desired accuracy is reached. In order to proceed we choose a generic resolution variable $\mathcal{T}_N$ and split the first addend of eq. (2.3) by means of a $\mathcal{T}_N^{\mathrm{cut}}$. Any resolution variable can be used, provided that $\mathcal{T}_N(\Phi_N) \equiv 0$ and that $\mathcal{T}_N(\Phi_{N+M}) \to 0$ in any infrared (IR) limit when the Φ_{N+M} configuration approaches Φ_N. Typical examples of such resolution variables are the transverse momentum of the colour singlet q_T for colour-singlet production or N-jettiness for

[1]Throughout this paper, we adopt the point of view of dressing a Born configuration with higher-order splittings, rather than starting from real emission diagrams and map them to a Born kinematics. The notation $\mathrm{d}\Phi_{N+k}/\mathrm{d}\Phi_N$ is thus a shorthand notation for the radiation phase space with k additional emissions at fixed underlying-Born kinematics. For example

$$\int\frac{\mathrm{d}\Phi_{N+1}}{\mathrm{d}\Phi_N} = \int\mathrm{d}\Phi_{N+1}\;\delta\left(\widetilde{\Phi}_N(\Phi_{N+1}) - \Phi_N\right)\,,$$

and $\widetilde{\Phi}_N(\Phi_{N+1})$ represent any possible projection of the $N+1$-body phase-space on the underlying-Born one Φ_N.

JHEP01(2026)065

processes that also include jets. Using the resolution cut, we can therefore rewrite

$$\begin{aligned}\mathcal{O}_{\delta\mathrm{NNLO}}(\Phi_N) = &\frac{\mathrm{d}\Sigma_N^{\delta\mathrm{NNLO}}}{\mathrm{d}\Phi_N}(\mathcal{T}_N^{\mathrm{cut}})\,\mathcal{O}(\Phi_N) \\ &+ \int \frac{\mathrm{d}\Phi_{N+1}}{\mathrm{d}\Phi_N}\frac{\mathrm{d}\sigma_{N+1}^{\delta\mathrm{NLO}}}{\mathrm{d}\Phi_{N+1}}\,\mathcal{O}(\Phi_N)\,\theta(\mathcal{T}_N(\Phi_{N+X}) > \mathcal{T}_N^{\mathrm{cut}}) \\ &+ \int \frac{\mathrm{d}\Phi_{N+1}}{\mathrm{d}\Phi_N}\frac{\mathrm{d}\sigma_{N+1}^{\delta\mathrm{NLO}}}{\mathrm{d}\Phi_{N+1}}\Big[\mathcal{O}(\Phi_{N+X}) - \mathcal{O}(\Phi_N)\Big]\,,\end{aligned} \tag{2.4}$$

where we have defined the cumulant below $\mathcal{T}_N^{\mathrm{cut}}$ as

$$\begin{aligned}\frac{\mathrm{d}\Sigma_N^{\delta\mathrm{NNLO}}}{\mathrm{d}\Phi_N}(\mathcal{T}_N^{\mathrm{cut}}) &= W(\Phi_N) + \int \frac{\mathrm{d}\Phi_{N+1}}{\mathrm{d}\Phi_N} RV(\Phi_{N+1})\theta(\mathcal{T}_N(\Phi_{N+1}) < \mathcal{T}_N^{\mathrm{cut}}) \\ &\quad + \int \frac{\mathrm{d}\Phi_{N+2}}{\mathrm{d}\Phi_N} RR(\Phi_{N+2})\theta(\mathcal{T}_N(\Phi_{N+2}) < \mathcal{T}_N^{\mathrm{cut}}) \\ &= \int_0^{\mathcal{T}_N^{\mathrm{cut}}} \mathrm{d}\mathcal{T}_N\,\frac{\mathrm{d}\sigma_N^{\delta\mathrm{NNLO}}}{\mathrm{d}\Phi_N\,\mathrm{d}\mathcal{T}_N}\,,\end{aligned} \tag{2.5}$$

and the $\mathcal{T}_N$ spectrum as

$$\begin{aligned}\frac{\mathrm{d}\sigma_N^{\delta\mathrm{NNLO}}}{\mathrm{d}\Phi_N\,\mathrm{d}\mathcal{T}_N} &= W(\Phi_N)\delta(\mathcal{T}_N) + \int \frac{\mathrm{d}\Phi_{N+1}}{\mathrm{d}\Phi_N} RV(\Phi_{N+1})\delta(\mathcal{T}_N(\Phi_{N+1}) - \mathcal{T}_N) \\ &\quad + \int \frac{\mathrm{d}\Phi_{N+2}}{\mathrm{d}\Phi_N} RR(\Phi_{N+2})\delta(\mathcal{T}_N(\Phi_{N+2}) - \mathcal{T}_N)\,.\end{aligned} \tag{2.6}$$

In the second line of eq. (2.4) we have again replaced the NNLO correction cross section above $\mathcal{T}_N^{\mathrm{cut}}$ by the cross section of the NLO corrections for one extra parton, integrated over the additional phase space, since the two are identical by definition. We can now add and subtract a "subtraction" cross section

$$\frac{\mathrm{d}\Sigma_{N,\mathrm{sub.}}^{\delta\mathrm{NNLO}}}{\mathrm{d}\Phi_N}(\mathcal{T}_N^{\mathrm{cut}}) = \int_0^{\mathcal{T}_N^{\mathrm{cut}}} \mathrm{d}\mathcal{T}_N\,\frac{\mathrm{d}\sigma_{N,\mathrm{sub.}}^{\delta\mathrm{NNLO}}}{\mathrm{d}\Phi_N\,\mathrm{d}\mathcal{T}_N}\,, \tag{2.7}$$

and obtain

$$\begin{aligned}\mathcal{O}_{\delta\mathrm{NNLO}}(\Phi_N) = &\frac{\mathrm{d}\Sigma_{N,\mathrm{sub.}}^{\delta\mathrm{NNLO}}}{\mathrm{d}\Phi_N}(\mathcal{T}_N^{\mathrm{cut}})\,\mathcal{O}(\Phi_N) \\ &+ \int \mathrm{d}\mathcal{T}_N\left[\frac{\mathrm{d}\sigma_N^{\delta\mathrm{NNLO}}}{\mathrm{d}\Phi_N\,\mathrm{d}\mathcal{T}_N} - \frac{\mathrm{d}\sigma_{N,\mathrm{sub.}}^{\delta\mathrm{NNLO}}}{\mathrm{d}\Phi_N\,\mathrm{d}\mathcal{T}_N}\right]\,\mathcal{O}(\Phi_N)\,\theta(\mathcal{T}_N < \mathcal{T}_N^{\mathrm{cut}}) \\ &+ \int \frac{\mathrm{d}\Phi_{N+1}}{\mathrm{d}\Phi_N}\frac{\mathrm{d}\sigma_{N+1}^{\delta\mathrm{NLO}}}{\mathrm{d}\Phi_{N+1}}\,\mathcal{O}(\Phi_N)\,\theta(\mathcal{T}_N(\Phi_{N+X}) > \mathcal{T}_N^{\mathrm{cut}}) \\ &+ \int \frac{\mathrm{d}\Phi_{N+1}}{\mathrm{d}\Phi_N}\frac{\mathrm{d}\sigma_{N+1}^{\delta\mathrm{NLO}}}{\mathrm{d}\Phi_{N+1}}\Big[\mathcal{O}(\Phi_{N+X}) - \mathcal{O}(\Phi_N)\Big]\,.\end{aligned} \tag{2.8}$$

The "subtraction" cross section can be chosen to be any valid approximation of the exact NNLO result. The minimum requirement is that it must include the leading-power (LP) singular contributions in $\mathcal{T}_N$, while it may also incorporate subleading-power corrections. The crucial point is that it has to reproduce at least the same singular structure in the variable

JHEP01(2026)065

$\mathcal{T}_N$ of the full δNNLO. We stress that the value of $\mathcal{T}_N^{\rm cut}$ is completely arbitrary up to this point and eq. (2.8) does not contain any approximation. It is however useful to introduce a tiny IR cutoff $\mathcal{T}_\delta \ll \mathcal{T}_N^{\rm cut}$ which we use to split the second line of eq. (2.8) into

$$\begin{aligned}\mathcal{O}_{\delta\rm NNLO}(\Phi_N) = &\frac{\mathrm{d}\Sigma^{\delta\rm NNLO}_{N,\rm sub.}}{\mathrm{d}\Phi_N}(\mathcal{T}_N^{\rm cut})\,\mathcal{O}(\Phi_N) \\ &+\int \mathrm{d}\mathcal{T}_N \left[\frac{\mathrm{d}\sigma^{\delta\rm NNLO}_N}{\mathrm{d}\Phi_N\,\mathrm{d}\mathcal{T}_N} - \frac{\mathrm{d}\sigma^{\delta\rm NNLO}_{N,\rm sub.}}{\mathrm{d}\Phi_N\,\mathrm{d}\mathcal{T}_N}\right]\,\mathcal{O}(\Phi_N)\,\theta(\mathcal{T}_N < \mathcal{T}_\delta) \\ &+\int \mathrm{d}\mathcal{T}_N \left[\frac{\mathrm{d}\sigma^{\delta\rm NNLO}_N}{\mathrm{d}\Phi_N\,\mathrm{d}\mathcal{T}_N} - \frac{\mathrm{d}\sigma^{\delta\rm NNLO}_{N,\rm sub.}}{\mathrm{d}\Phi_N\,\mathrm{d}\mathcal{T}_N}\right]\,\mathcal{O}(\Phi_N)\,\theta(\mathcal{T}_\delta < \mathcal{T}_N < \mathcal{T}_N^{\rm cut}) \\ &+\int \frac{\mathrm{d}\Phi_{N+1}}{\mathrm{d}\Phi_N}\frac{\mathrm{d}\sigma^{\delta\rm NLO}_{N+1}}{\mathrm{d}\Phi_{N+1}}\,\mathcal{O}(\Phi_N)\,\theta(\mathcal{T}_N(\Phi_{N+X}) > \mathcal{T}_N^{\rm cut}) \\ &+\int \frac{\mathrm{d}\Phi_{N+1}}{\mathrm{d}\Phi_N}\frac{\mathrm{d}\sigma^{\delta\rm NLO}_{N+1}}{\mathrm{d}\Phi_{N+1}}\Big[\mathcal{O}(\Phi_{N+X}) - \mathcal{O}(\Phi_N)\Big]\,.\end{aligned} \tag{2.9}$$

We now observe that due to the presence of the lower IR cutoff $\mathcal{T}_\delta$ that regulates any possible divergence in $\mathcal{T}_N$, the third line can again be rewritten using the NLO corrections for one extra parton integrated over the additional phase space. The same can also be done for the "subtraction" cross section, but here one needs to introduce some splitting function $P(\Phi_{N+1}) \propto \mathrm{d}\Phi_N \mathrm{d}\mathcal{T}_N/\mathrm{d}\Phi_{N+1}$ to make the "subtraction" cross section differential in the Φ_{N+1} phase space. For a generic function $f(\Phi_N, \mathcal{T}_N)$ the splitting functions have to obey the normalization relation

$$f(\Phi_N, \mathcal{T}_N) = \int \frac{\mathrm{d}\Phi_{N+1}}{\mathrm{d}\Phi_N} f(\Phi_N, \mathcal{T}_N) P(\Phi_{N+1})\,, \tag{2.10}$$

that ensures that the subtraction remains local in the $\mathcal{T}_N$ variable. Eventually we obtain

$$\begin{aligned}\mathcal{O}_{\delta\rm NNLO}(\Phi_N) = &\frac{\mathrm{d}\Sigma^{\delta\rm NNLO}_{N,\rm sub.}}{\mathrm{d}\Phi_N}(\mathcal{T}_N^{\rm cut})\,\mathcal{O}(\Phi_N) \\ &+\int \mathrm{d}\mathcal{T}_N \left[\frac{\mathrm{d}\sigma^{\delta\rm NNLO}_N}{\mathrm{d}\Phi_N\,\mathrm{d}\mathcal{T}_N} - \frac{\mathrm{d}\sigma^{\delta\rm NNLO}_{N,\rm sub.}}{\mathrm{d}\Phi_N\,\mathrm{d}\mathcal{T}_N}\right]\,\mathcal{O}(\Phi_N)\,\theta(\mathcal{T}_N < \mathcal{T}_\delta) \\ &+\int \frac{\mathrm{d}\Phi_{N+1}}{\mathrm{d}\Phi_N}\left[\frac{\mathrm{d}\sigma^{\delta\rm NLO}_{N+1}}{\mathrm{d}\Phi_{N+1}} - \frac{\mathrm{d}\sigma^{\delta\rm NNLO}_{N,\rm sub.}}{\mathrm{d}\Phi_N\,\mathrm{d}\mathcal{T}_N}\,P(\Phi_{N+1})\,\theta(\mathcal{T}_N(\Phi_{N+1}) < \mathcal{T}_N^{\rm cut})\right] \\ &\qquad\qquad \times \mathcal{O}(\Phi_N)\,\theta(\mathcal{T}_N(\Phi_{N+X}) > \mathcal{T}_\delta) \\ &+\int \frac{\mathrm{d}\Phi_{N+1}}{\mathrm{d}\Phi_N}\frac{\mathrm{d}\sigma^{\delta\rm NLO}_{N+1}}{\mathrm{d}\Phi_{N+1}}\Big[\mathcal{O}(\Phi_{N+X}) - \mathcal{O}(\Phi_N)\Big]\,.\end{aligned} \tag{2.11}$$

We remark that no approximation went in the derivation up to now, and all the terms in the equation above are exactly calculable down to the value of $\mathcal{T}_N$ reaching zero, because either the divergences are subtracted by an approximate δNNLO correction as in the second line or by the difference of the observables as in the last line (which ensures finiteness for any IR safe observable by the KLN theorem). By inspecting the third line of eq. (2.11) the complementary role of the cuts on $\mathcal{T}_N$ becomes clear: $\mathcal{T}_N^{\rm cut}$ is an upper limit on the range where the "subtraction" cross section is applied, while $\mathcal{T}_\delta$ acts as the true lower IR

JHEP01(2026)065

cutoff. When they are taken equal the subtraction region shrinks to zero and one is back to the traditional slicing approach.

The inclusion of the subtraction in the $\mathcal{T}_N$ spectrum is particularly delicate in the presence of generating cuts, that serve to keep the cross section finite over singular regions in the underlying-Born phase space. Because of these extra conditions, the choice of the phase-space mappings used in the calculation of the NLO cross section $\mathrm{d}\sigma^{\delta\mathrm{NLO}}_{N+1}/\mathrm{d}\Phi_{N+1}$ or in the splitting functions $P(\Phi_{N+1})$ requires particular attention. Complete freedom over the choice of the mapping in NLO cross section is still guaranteed, provided that the mismatch generated by mappings that do not preserve the generating cuts is accounted for. Instead, only by preserving the generating cuts in the mappings used for the splitting functions one can ensure that the entirety of the allowed phase space is correctly covered, and the correct predictions are obtained. This will be further discussed in section 3.

At this point we are ready to discuss which terms to drop from eq. (2.11) and the corresponding approximation. By dropping the second line we are neglecting the subleading inclusive power corrections below the $\mathcal{T}_\delta$ tiny cutoff, and only those. Indeed, since the observable is always evaluated on the underlying-Born kinematics in that line, there are no missing FPCs. The FPCs below the $\mathcal{T}_\delta$ tiny cutoff are instead included by evaluating the NLO corrections for one extra jet down $\mathcal{T}_N = 0$, as done in the last line of eq. (2.11). This is possible because the divergences of the cross-section are regulated by the difference in the observable. Highlighting again that the only approximation is neglecting the inclusive power corrections below the infrared cutoff $\mathcal{T}_\delta$, our final formula is

$$
\begin{aligned}
\mathcal{O}_{\delta\mathrm{NNLO}}(\Phi_N) = {} & \frac{\mathrm{d}\Sigma^{\delta\mathrm{NNLO}}_{N,\mathrm{sub.}}}{\mathrm{d}\Phi_N}(\mathcal{T}_N^{\mathrm{cut}})\,\mathcal{O}(\Phi_N) \\
& + \int \frac{\mathrm{d}\Phi_{N+1}}{\mathrm{d}\Phi_N}\left[\frac{\mathrm{d}\sigma^{\delta\mathrm{NLO}}_{N+1}}{\mathrm{d}\Phi_{N+1}} - \frac{\mathrm{d}\sigma^{\delta\mathrm{NNLO}}_{N,\mathrm{sub.}}}{\mathrm{d}\Phi_N\,\mathrm{d}\mathcal{T}_N}\,P(\Phi_{N+1})\,\theta(\mathcal{T}_N(\Phi_{N+1}) < \mathcal{T}_N^{\mathrm{cut}})\right] \\
& \qquad \times \mathcal{O}(\Phi_N)\;\theta(\mathcal{T}_N(\Phi_{N+X}) > \mathcal{T}_\delta) \\
& + \int \frac{\mathrm{d}\Phi_{N+1}}{\mathrm{d}\Phi_N}\frac{\mathrm{d}\sigma^{\delta\mathrm{NLO}}_{N+1}}{\mathrm{d}\Phi_{N+1}}\Big[\mathcal{O}(\Phi_{N+X}) - \mathcal{O}(\Phi_N)\Big] \\
& + \text{neglected inclusive power corrections in } \mathcal{T}_\delta\,.
\end{aligned}
\tag{2.12}
$$

The size of the neglected inclusive power corrections can be controlled by the choice of the subtraction cross section used. The simplest choice is to use the singular cumulant at relative order α_s^2 for $\mathrm{d}\Sigma^{\delta\mathrm{NNLO}}_{N,\mathrm{sub.}}/\mathrm{d}\Phi_N$, i.e. including only the leading-power contributions. This can however be ameliorated by adding further subleading power terms. For example, including the subleading-power leading logarithms one can make the inclusive power corrections in $\mathcal{T}_\delta$ in the last line smaller. The choice of the subtraction cross section cumulant in the first line determines the choice the subtraction spectrum appearing in the second line. Ultimately this determines the associated nonsingular spectrum, i.e. the difference between the full NLO result and its singular approximation, differential in $\mathcal{T}_N$ and obtained via a subtraction. Here the keys to obtain stable and rapidly converging results are the mapping that is used in the NLO calculation and the splitting function that is used in the "subtraction" part. The less the observable is modified between the Φ_{N+1} or Φ_{N+2} phase spaces and the underlying-Born Φ_N one, the more stable and more rapidly converging the results will be.

JHEP01(2026)065

We remark that in order for the subtraction to be as local as possible eq. (2.12) requires the contribution $-\mathrm{d}\sigma^{\delta\mathrm{NNLO}}_{N,\mathrm{sub.}}/(\mathrm{d}\Phi_N \mathrm{d}\mathcal{T}_N)\ P(\Phi_{N+1})$ to approximate as much as possible the sum of the real-virtual and the double real contributions, not only in the $\mathcal{T}_N$ variable but also in the flavour indexes, which are omitted in the previous formulae. This is quite nontrivial to obtain at $\mathcal{O}(\alpha_s^2)$, given that the subtraction term is usually obtained by the singular spectrum which is summed over the possible flavours and partonic channels, and in order to make it differential over the flavours again one would have to devise splitting functions which carry the correct $\mathcal{T}_N$ and flavour dependence at $\mathcal{O}(\alpha_s^2)$.

The third line of eq. (2.12) is just the difference between the NLO corrections of the cross-section with one extra jet for the observable evaluated on the exact or projected kinematics, over the entirety of the phase space. The mapping used in this projection also plays an important role in obtaining rapidly converging results in the P2B method. The consequences of these choices are further discussed in section 3.4.

In general the value of $\mathcal{T}_N^{\mathrm{cut}}$ can be freely taken and the result is independent from this choice due to the compensating effect between the first and the second line. It is however better to choose a value that makes those two compensating terms roughly of the same size, in order to minimize the numerical errors in the combination. The value of $\mathcal{T}_\delta$ must instead be chosen as small as permitted by the stability of the NLO calculation above it, in order to make the neglected inclusive power corrections as small as possible.

3 Implementation details

In this section we discuss the implementation of eq. (2.12) into the GENEVA code, also including the fiducial power corrections below the $\mathcal{T}_\delta$ tiny cutoff. We start by reminding the reader that $\mathrm{d}\sigma^{\delta\mathrm{NLO}}_{N+1}/\mathrm{d}\Phi_{N+1}\ \mathcal{O}(\Phi_{N+X})$ is in general not known analytically and must therefore be obtained numerically using a NLO local subtraction. This is achieved in GENEVA with the FKS subtraction method [84, 85]. Omitting counterterms for ease of notation this reads

$$\frac{\mathrm{d}\sigma^{\delta\mathrm{NLO}}_{N+1}}{\mathrm{d}\Phi_{N+1}}\ \mathcal{O}(\Phi_{N+X}) = R\!\!V(\Phi_{N+1})\mathcal{O}(\Phi_{N+1}) + \int \frac{\mathrm{d}\Phi_{N+2}}{\mathrm{d}\Phi_{N+1}} RR(\Phi_{N+2})\mathcal{O}(\Phi_{N+2})\,. \tag{3.1}$$

In GENEVA, the real corrections of the NLO_{N+1} calculation are separated according to the value of $\mathcal{T}_{N+1}(\Phi_{N+2})$ into different *jet bins* contributions using the resolution cutoff $\mathcal{T}_{N+1}^{\mathrm{cut}}$, depending if $\mathcal{T}_{N+1}(\Phi_{N+2}) < \mathcal{T}_{N+1}^{\mathrm{cut}}$ or not. In order to cover the phase space entirely, the nonsingular and nonprojectable contributions from the Φ_{N+2} phase space with $\mathcal{T}_{N+1}(\Phi_{N+2}) < \mathcal{T}_{N+1}^{\mathrm{cut}}$, which are not obtainable through a splitting of Φ_{N+1} phase space below the resolution cutoff, are included in the $N+2$ jet bin. We indeed partition the part of the Φ_{N+2} phase space which is not removed by the process-defining cuts with a set of mutually exclusive jet-bin theta functions $\Theta_{N+1}(\Phi_{N+2})\,, \Theta_{N+2}(\Phi_{N+2})$, which obey $\Theta_{N+1}(\Phi_{N+2}) + \Theta_{N+2}(\Phi_{N+2}) \equiv 1$. The latter, $\Theta_{N+2}(\Phi_{N+2})$ corresponds to

$$\Theta_{N+2}(\Phi_{N+2}) = \theta(\mathcal{T}_{N+1}(\Phi_{N+2}) > \mathcal{T}_{N+1}^{\mathrm{cut}}) \ + \ \bar{\Theta}_{\mathrm{flav.}}(\Phi_{N+2}) \ + \ \bar{\Theta}_{\mathrm{map}}(\Phi_{N+2})\,, \tag{3.2}$$

where $\bar{\Theta}_{\mathrm{flav.}}$ and $\bar{\Theta}_{\mathrm{map}}$ represent invalid flavour and map projection of the two-closest partons, respectively. These correspond to configurations which are nonsingular in $\mathcal{T}_{N+1}$ (despite also

JHEP01(2026)065

having $\mathcal{T}_{N+1}(\Phi_{N+2}) < \mathcal{T}_{N+1}^{\text{cut}}$). A map projection can be invalid, e.g., if the map does not cover the entirety of the phase space. The former, $\Theta_{N+1}(\Phi_{N+2})$ is instead the complement of Θ_{N+2} in the region which is not removed by the process-defining cuts (and not the complement of the whole Φ_{N+2} in general)

$$\Theta_{N+1}(\Phi_{N+2}) = \theta(\mathcal{T}_{N+1}(\Phi_{N+2}) < \mathcal{T}_{N+1}^{\text{cut}}) \times \Theta_{\text{flav.}}(\Phi_{N+2}) \times \Theta_{\text{map}}(\Phi_{N+2}) \,. \tag{3.3}$$

This is implemented through a combination of restrictions on the Φ_{N+1} phase space and on the splitting $\Phi_{N+1} \to \Phi_{N+2}$ that ensures unitarity within the generation cuts, cfr. section 3.2. Expressing the NLO_{N+1} corrections in terms of their actual contributions and taking also into account eqs. (3.2) and (3.3), we can rewrite eq. (2.12), after some simple manipulation, as follows

$$\begin{aligned}
\mathcal{O}_{\delta\text{NNLO}}(\Phi_N) = {} & \frac{\mathrm{d}\Sigma_{N,\text{sub.}}^{\delta\text{NNLO}}}{\mathrm{d}\Phi_N}(\mathcal{T}_N^{\text{cut}})\,\mathcal{O}(\Phi_N) \\
& + \Bigg\{ \int \frac{\mathrm{d}\Phi_{N+1}}{\mathrm{d}\Phi_N}\,\theta(\mathcal{T}_N(\Phi_{N+1}) > \mathcal{T}_\delta) \Big[RV(\Phi_{N+1}) \\
& \quad + \int \frac{\mathrm{d}\Phi_{N+2}}{\mathrm{d}\Phi_{N+1}} [RR\;\Theta_{N+1}](\Phi_{N+2})\,\theta(\mathcal{T}_N(\Phi_{N+2}) > \mathcal{T}_\delta) \\
& \quad - \frac{\mathrm{d}\sigma_{N,\text{sub.}}^{\delta\text{NNLO}}}{\mathrm{d}\Phi_N \mathrm{d}\mathcal{T}_N}\,P(\Phi_{N+1})\,\theta(\mathcal{T}_N(\Phi_{N+1}) < \mathcal{T}_N^{\text{cut}}) \Big] \\
& \quad + \int \frac{\mathrm{d}\Phi_{N+2}}{\mathrm{d}\Phi_N} \Big[[RR\;\Theta_{N+1}](\Phi_{N+2})\,\theta(\mathcal{T}_N(\widetilde{\Phi}_{N+1}) < \mathcal{T}_\delta) \\
& \quad\quad + [RR\;\Theta_{N+2}](\Phi_{N+2}) \Big]\,\theta(\mathcal{T}_N(\Phi_{N+2}) > \mathcal{T}_\delta) \Bigg\}\,\mathcal{O}(\Phi_N) \\
& + \int \frac{\mathrm{d}\Phi_{N+1}}{\mathrm{d}\Phi_N} \Big[RV(\Phi_{N+1}) [\mathcal{O}(\Phi_{N+1}) - \mathcal{O}(\Phi_N)] \\
& \quad + \int \frac{\mathrm{d}\Phi_{N+2}}{\mathrm{d}\Phi_{N+1}} [RR\;\Theta_{N+1}](\Phi_{N+2}) [\mathcal{O}(\Phi_{N+2}) - \mathcal{O}(\Phi_N)] \Big] \\
& + \int \frac{\mathrm{d}\Phi_{N+2}}{\mathrm{d}\Phi_N} [RR\;\Theta_{N+2}](\Phi_{N+2}) [\mathcal{O}(\Phi_{N+2}) - \mathcal{O}(\Phi_N)] \,.
\end{aligned} \tag{3.4}$$

This formula is better adapted to the internal structure of GENEVA, in particular separating the integration of the Φ_{N+2} phase space points that are directly obtained from the phase space generator from the ones that are obtained through a $\Phi_{N+1} \to \Phi_{N+2}$ splitting, which are sampled differently. In the fifth line of eq. (3.4) the $\theta(\mathcal{T}_N(\widetilde{\Phi}_{N+1}) < \mathcal{T}_\delta)$ term is evaluated on a projected $\Phi_{N+2} \to \widetilde{\Phi}_{N+1}$ point, which is in general different from the Φ_{N+1} generated point. This contribution adds back the Φ_{N+2} points with $\theta(\mathcal{T}_N(\Phi_{N+2}) > \mathcal{T}_\delta)$ that cannot be generated via the $\Phi_{N+1} \to \Phi_{N+2}$ splitting because they fail the initial condition $\theta(\mathcal{T}_N(\Phi_{N+1}) > \mathcal{T}_\delta)$ before the splitting. Obviously, choosing a splitting and a projection that preserve the value of $\mathcal{T}_N$ will remove this additional contribution. This complication is not present in the last three lines featuring the P2B subtraction because the IR cutoff $\mathcal{T}_\delta$ is not required there. This means that the real-virtual and double real contributions are evaluated without a lower cutoff, but they are contributing only when the difference between the observable evaluated on the exact or projected kinematics is non vanishing.

JHEP01(2026)065

3.1 Exclusion of fiducial power corrections

For completeness we also present the formula that one obtains when we do not exploit the P2B method and neglect the FPCs:

$$\begin{aligned}\mathcal{O}_{\delta\mathrm{NNLO}}(\Phi_N) = &\frac{\mathrm{d}\Sigma^{\delta\mathrm{NNLO}}_{N,\mathrm{sub.}}}{\mathrm{d}\Phi_N}(\mathcal{T}_N^{\mathrm{cut}})\,\mathcal{O}(\Phi_N) \\ &+\int\frac{\mathrm{d}\Phi_{N+1}}{\mathrm{d}\Phi_N}\,\theta(\mathcal{T}_N(\Phi_{N+1})>\mathcal{T}_\delta)\,\Big[RV(\Phi_{N+1})\mathcal{O}(\Phi_{N+1}) \\ &\quad+\int\frac{\mathrm{d}\Phi_{N+2}}{\mathrm{d}\Phi_{N+1}}\big[RR\;\Theta_{N+1}\big](\Phi_{N+2})\mathcal{O}(\Phi_{N+2})\theta(\mathcal{T}_N(\Phi_{N+2})>\mathcal{T}_\delta) \\ &\quad-\frac{\mathrm{d}\sigma^{\delta\mathrm{NNLO}}_{N,\mathrm{sub.}}}{\mathrm{d}\Phi_N\mathrm{d}\mathcal{T}_N}\,P(\Phi_{N+1})\mathcal{O}(\Phi_N)\theta(\mathcal{T}_N(\Phi_{N+1})<\mathcal{T}_N^{\mathrm{cut}})\Big] \\ &+\int\frac{\mathrm{d}\Phi_{N+2}}{\mathrm{d}\Phi_N}\Big[\big[RR\;\Theta_{N+1}\big](\Phi_{N+2})\;\theta(\mathcal{T}_N(\widetilde{\Phi}_{N+1})<\mathcal{T}_\delta) \\ &\quad+\big[RR\;\Theta_{N+2}\big](\Phi_{N+2})\Big]\;\mathcal{O}(\Phi_{N+2})\;\theta(\mathcal{T}_N(\Phi_{N+2})>\mathcal{T}_\delta)\,.\end{aligned} \tag{3.5}$$

This is not the default, because in general one pays the price of reintroducing observable-depend power corrections below $\mathcal{T}_\delta$, but in case one is interested in evaluating inclusive observables (or those preserved by the P2B mapping) that do not suffer from FPCs, it is better for numerical efficiency to use the simpler formula above that avoids evaluating quantities that are eventually canceled.

3.2 Inclusion of restrictions at the generation level

For some processes we need to impose process-defining phase space restrictions $\Theta^{\mathrm{PS}}(\Phi_N)$ in order to have a finite cross section already at the leading order. We collective call this restriction as *generation cuts* even if their actual formulation could be more complicated than just a simple cut on some variable. For example, for processes with final-state photons the appropriate restriction might involve some photon isolation procedure. These generation cuts affect our formulae as explained in the following. Additionally, we use the symbol $\Theta^{\mathrm{PS}}_{\mathrm{proj}}(\widetilde{\Phi}_{N+1})$ (and $\overline{\Theta}^{\mathrm{PS}}_{\mathrm{proj}}(\widetilde{\Phi}_{N+1})$ for its complement) to indicate this set of phase space restrictions acting on the higher dimensional Φ_{N+2} phase space due to the cuts on the projected configuration $\widetilde{\Phi}_{N+1}$. In practice, this means that when a term in the cross section, evaluated at a Φ_{N+2} phase space point, is multiplied by $\Theta^{\mathrm{PS}}_{\mathrm{proj}}(\widetilde{\Phi}_{N+1})$, the Φ_{N+2} phase space point is projected onto a $\widetilde{\Phi}_{N+1}$ point and the cuts are applied on this lower dimensional space. If the projected configuration does not pass the cuts, the initial Φ_{N+2} configuration is excluded. Notice that the separation realized by the introduction of $\Theta^{\mathrm{PS}}_{\mathrm{proj}}$ and $\overline{\Theta}^{\mathrm{PS}}_{\mathrm{proj}}$ is only required in our implementation of the fixed-order calculation because of the choice of generating the Φ_{N+2} phase space starting from Φ_{N+1} satisfying $\Theta^{\mathrm{PS}}(\Phi_{N+1})$ instead of starting from all Φ_{N+1} points. In order to keep the formulae simpler we continue to only consider observables that

JHEP01(2026)065

are not affected by FPCs; we will comment on how to extend these results to include FPCs in section 3.4. In this case eq. (3.5) becomes

$$\begin{aligned}\mathcal{O}_{\delta\text{NNLO}}(\Phi_N) = &\frac{\mathrm{d}\Sigma^{\delta\text{NNLO}}_{N,\text{sub.}}}{\mathrm{d}\Phi_N}(\mathcal{T}_N^{\text{cut}})\Theta^{\text{PS}}(\Phi_N)\,\mathcal{O}(\Phi_N) \\ &+\int\frac{\mathrm{d}\Phi_{N+1}}{\mathrm{d}\Phi_N}\,\theta(\mathcal{T}_N(\Phi_{N+1})>\mathcal{T}_\delta)\,\Big[RV(\Phi_{N+1})\Theta^{\text{PS}}(\Phi_{N+1})\mathcal{O}(\Phi_{N+1}) \\ &\quad+\int\frac{\mathrm{d}\Phi_{N+2}}{\mathrm{d}\Phi_{N+1}}\big[RR\;\Theta_{N+1}\Theta^{\text{PS}}\big](\Phi_{N+2})\Theta^{\text{PS}}_{\text{proj}}(\widetilde{\Phi}_{N+1})\mathcal{O}(\Phi_{N+2})\theta(\mathcal{T}_N(\Phi_{N+2})>\mathcal{T}_\delta) \\ &\quad-\frac{\mathrm{d}\sigma^{\delta\text{NNLO}}_{N,\text{sub.}}}{\mathrm{d}\Phi_N\mathrm{d}\mathcal{T}_N}\,P(\Phi_{N+1})\Theta^{\text{PS}}(\Phi_N)\mathcal{O}(\Phi_N)\theta(\mathcal{T}_N(\Phi_{N+1})<\mathcal{T}_N^{\text{cut}})\Big] \\ &+\int\frac{\mathrm{d}\Phi_{N+2}}{\mathrm{d}\Phi_N}\Big[\big[RR\;\Theta_{N+1}\Theta^{\text{PS}}\big](\Phi_{N+2})\Big(\overline{\Theta}^{\text{PS}}_{\text{proj}}(\widetilde{\Phi}_{N+1})+\theta(\mathcal{T}_N(\widetilde{\Phi}_{N+1})<\mathcal{T}_\delta)\Big) \\ &\quad+\big[RR\;\Theta_{N+2}\Theta^{\text{PS}}\big](\Phi_{N+2})\Big]\,\mathcal{O}(\Phi_{N+2})\theta(\mathcal{T}_N(\Phi_{N+2})>\mathcal{T}_\delta)\,.\end{aligned} \tag{3.6}$$

In the equation above, the $\overline{\Theta}^{\text{PS}}_{\text{proj}}(\widetilde{\Phi}_{N+1})$ in the second-to-last line correctly reinstates the Φ_{N+2} contributions that could not be generated via a $\Phi_{N+1}\to\Phi_{N+2}$ splitting because of the phase space restriction $\Theta^{\text{PS}}(\Phi_{N+1})$. It is also important to notice that the $\Theta^{\text{PS}}(\Phi_N)$ multiplying the splitting function $P(\Phi_{N+1})$ should be instead a $\Theta^{\text{PS}}(\Phi_{N+1})$, because that is the actual cut on the generated points. However, if one makes that choice the relation connecting the integral of the spectrum $\mathrm{d}\sigma^{\delta\text{NNLO}}_{N,\text{sub.}}$ between $\mathcal{T}_\delta$ and $\mathcal{T}_N^{\text{cut}}$ and the cumulant $\mathrm{d}\Sigma^{\delta\text{NNLO}}_{N,\text{sub.}}$ above $\mathcal{T}_\delta$ is violated, resulting a miscancellation of the subtraction term. This problem can be avoided only if the mapping used in the splitting functions preserves the process defining cuts, such that one can safely make the replacement $\Theta^{\text{PS}}(\Phi_{N+1}) = \Theta^{\text{PS}}(\Phi_N)$. Factoring out the restrictions at the generation level, eq. (3.6) can be written as

$$\begin{aligned}\mathcal{O}_{\delta\text{NNLO}}(\Phi_N) = &\frac{\mathrm{d}\Sigma^{\delta\text{NNLO}}_{N,\text{sub.}}}{\mathrm{d}\Phi_N}(\mathcal{T}_N^{\text{cut}})\Theta^{\text{PS}}(\Phi_N)\,\mathcal{O}(\Phi_N) \\ &+\int\frac{\mathrm{d}\Phi_{N+1}}{\mathrm{d}\Phi_N}\Theta^{\text{PS}}(\Phi_{N+1})\theta(\mathcal{T}_N(\Phi_{N+1})>\mathcal{T}_\delta)\,\Big[RV(\Phi_{N+1})\mathcal{O}(\Phi_{N+1}) \\ &\quad+\int\frac{\mathrm{d}\Phi_{N+2}}{\mathrm{d}\Phi_{N+1}}\big[RR\;\Theta_{N+1}\Theta^{\text{PS}}\big](\Phi_{N+2})\mathcal{O}(\Phi_{N+2})\theta(\mathcal{T}_N(\Phi_{N+2})>\mathcal{T}_\delta) \\ &\quad-\frac{\mathrm{d}\sigma^{\delta\text{NNLO}}_{N,\text{sub.}}}{\mathrm{d}\Phi_N\mathrm{d}\mathcal{T}_N}\,P(\Phi_{N+1})\mathcal{O}(\Phi_N)\theta(\mathcal{T}_N(\Phi_{N+1})<\mathcal{T}_N^{\text{cut}})\Big] \\ &+\int\frac{\mathrm{d}\Phi_{N+2}}{\mathrm{d}\Phi_N}\Big[\big[RR\;\Theta_{N+1}\Theta^{\text{PS}}\big](\Phi_{N+2})\Big(\overline{\Theta}^{\text{PS}}_{\text{proj}}(\widetilde{\Phi}_{N+1})+\theta(\mathcal{T}_N(\widetilde{\Phi}_{N+1})<\mathcal{T}_\delta)\Big) \\ &\quad+\big[RR\;\Theta_{N+2}\Theta^{\text{PS}}\big](\Phi_{N+2})\Big]\,\mathcal{O}(\Phi_{N+2})\theta(\mathcal{T}_N(\Phi_{N+2})>\mathcal{T}_\delta)\,.\end{aligned} \tag{3.7}$$

3.3 Usage of dynamical cuts

When dealing with multi-scale processes, it may be advantageous to employ dynamical generation and resolution cuts to better capture the richer kinematic structures that could logarithmically enhance certain phase space regions. This is also more efficient from a

JHEP01(2026)065

numerical point of view: if the nonsingular contribution is not particularly enhanced in a corner of the phase space, the corresponding IR cutoff can safely be raised without paying too hefty a price in terms of missing power corrections. The increased IR cutoff delivers in turn much stabler fixed-order corrections. We express the dependence of the generation and resolution cuts on the generic phase space point though the substitutions $\mathcal{T}_\delta \to \mathcal{T}_\delta(\Phi_{N+X})$ and $\mathcal{T}_N^{\text{cut}} \to \mathcal{T}_N^{\text{cut}}(\Phi_{N+X})$, respectively, and we write

$$
\begin{aligned}
\mathcal{O}_{\delta\text{NNLO}}(\Phi_N) = {} & \frac{\mathrm{d}\Sigma^{\delta\text{NNLO}}_{N,\text{sub.}}}{\mathrm{d}\Phi_N}(\mathcal{T}_N^{\text{cut}}(\Phi_N))\Theta^{\text{PS}}(\Phi_N)\,\mathcal{O}(\Phi_N) \\
& + \int \frac{\mathrm{d}\Phi_{N+1}}{\mathrm{d}\Phi_N}\Bigg\{\Theta^{\text{PS}}(\Phi_{N+1})\theta(\mathcal{T}_N(\Phi_{N+1}) > \mathcal{T}_\delta(\Phi_{N+1}))\Bigg[RV(\Phi_{N+1})\mathcal{O}(\Phi_{N+1}) \\
& \quad + \int \frac{\mathrm{d}\Phi_{N+2}}{\mathrm{d}\Phi_{N+1}}\big[RR\;\Theta_{N+1}\Theta^{\text{PS}}\big](\Phi_{N+2})\mathcal{O}(\Phi_{N+2})\theta(\mathcal{T}_N(\Phi_{N+2}) > \mathcal{T}_\delta(\Phi_{N+2})) \\
& \quad - \frac{\mathrm{d}\sigma^{\delta\text{NNLO}}_{N,\text{sub.}}}{\mathrm{d}\Phi_N\mathrm{d}\mathcal{T}_N}\,P(\Phi_{N+1})\mathcal{O}(\Phi_N)\theta(\mathcal{T}_N(\Phi_{N+1}) < \mathcal{T}_N^{\text{cut}}(\Phi_{N+1}))\Bigg]\Bigg\} \\
& + \int \frac{\mathrm{d}\Phi_{N+2}}{\mathrm{d}\Phi_N}\Bigg[\big[RR\;\Theta_{N+1}\Theta^{\text{PS}}\big](\Phi_{N+2})\Big(\overline{\Theta}^{\text{PS}}_{\text{proj}}(\widetilde{\Phi}_{N+1}) + \theta(\mathcal{T}_N(\widetilde{\Phi}_{N+1}) < \mathcal{T}_\delta(\widetilde{\Phi}_{N+1}))\Big) \\
& \quad + \big[RR\;\Theta_{N+2}\Theta^{\text{PS}}\big](\Phi_{N+2})\Bigg]\,\mathcal{O}(\Phi_{N+2})\theta(\mathcal{T}_N(\Phi_{N+2}) > \mathcal{T}_\delta(\Phi_{N+2}))\,.
\end{aligned}
\tag{3.8}
$$

As done for eq. (3.7), this formula only works under the important assumption that the mapping used in the splitting functions preserves both the process defining cuts (as before) but now also the dynamical cuts, i.e. $\mathcal{T}_\delta(\Phi_{N+1}) = \mathcal{T}_\delta(\Phi_N)$ and $\mathcal{T}_N^{\text{cut}}(\Phi_{N+1}) = \mathcal{T}_N^{\text{cut}}(\Phi_N)$. Note that if the splitting mapping used in the NLO_{N+1} calculation does not preserve the defining functional dependence of $\mathcal{T}_\delta(\Phi_{N+2})$, in order to capture the points that were excluded before the splitting, the dynamic cutoff in the last line of (3.8) needs also to be evaluated on the projected configuration, $\mathcal{T}_\delta(\widetilde{\Phi}_{N+1})$, which can result in a different numerical value.

3.4 Mappings for the P2B method

At this point we are ready to discuss how the fiducial power corrections can be incorporated again, even in the presence of phase-space restrictions at the generation level and of dynamical cuts. Combining eq. (3.4) and eq. (3.8) we obtain

$$
\begin{aligned}
\mathcal{O}_{\delta\text{NNLO}}(\Phi_N) = {} & \Bigg\{\frac{\mathrm{d}\Sigma^{\delta\text{NNLO}}_{N,\text{sub.}}}{\mathrm{d}\Phi_N}(\mathcal{T}_N^{\text{cut}}(\Phi_N))\Theta^{\text{PS}}(\Phi_N) \\
& + \int \frac{\mathrm{d}\Phi_{N+1}}{\mathrm{d}\Phi_N}\Bigg\{\Theta^{\text{PS}}(\Phi_{N+1})\theta(\mathcal{T}_N(\Phi_{N+1}) > \mathcal{T}_\delta(\Phi_{N+1}))\Bigg[RV(\Phi_{N+1}) \\
& \quad + \int \frac{\mathrm{d}\Phi_{N+2}}{\mathrm{d}\Phi_{N+1}}\big[RR\;\Theta_{N+1}\Theta^{\text{PS}}\big](\Phi_{N+2})\theta(\mathcal{T}_N(\Phi_{N+2}) > \mathcal{T}_\delta(\Phi_{N+2})) \\
& \quad - \frac{\mathrm{d}\sigma^{\delta\text{NNLO}}_{N,\text{sub.}}}{\mathrm{d}\Phi_N\mathrm{d}\mathcal{T}_N}\,P(\Phi_{N+1})\theta(\mathcal{T}_N(\Phi_{N+1}) < \mathcal{T}_N^{\text{cut}}(\Phi_{N+1}))\Bigg]\Bigg\}
\end{aligned}
\tag{3.9}
$$

JHEP01(2026)065

$$
\begin{aligned}
&+\int \frac{\mathrm{d}\Phi_{N+2}}{\mathrm{d}\Phi_N}\Bigg[\big[RR\;\Theta_{N+1}\Theta^{\mathrm{PS}}\big](\Phi_{N+2})\Big(\overline{\Theta}^{\mathrm{PS}}_{\mathrm{proj}}(\widetilde{\Phi}_{N+1})+\theta\big(\mathcal{T}_N(\widetilde{\Phi}_{N+1})<\mathcal{T}_\delta(\widetilde{\Phi}_{N+1})\big)\Big)\\
&\quad+\big[RR\;\Theta_{N+2}\Theta^{\mathrm{PS}}\big](\Phi_{N+2})\Bigg]\theta\big(\mathcal{T}_N(\Phi_{N+2})>\mathcal{T}_\delta(\Phi_{N+2})\big)\Bigg\}\;\mathcal{O}(\Phi_N)\\
&+\int \frac{\mathrm{d}\Phi_{N+1}}{\mathrm{d}\Phi_N}\Theta^{\mathrm{PS}}(\Phi_{N+1})\Bigg[RV(\Phi_{N+1})\big[\mathcal{O}(\Phi_{N+1})-\mathcal{O}(\Phi_N)\big]\\
&\quad+\int \frac{\mathrm{d}\Phi_{N+2}}{\mathrm{d}\Phi_{N+1}}\big[RR\;\Theta_{N+1}\Theta^{\mathrm{PS}}\big](\Phi_{N+2})\big[\mathcal{O}(\Phi_{N+2})-\mathcal{O}(\Phi_N)\big]\Bigg]\\
&+\int \frac{\mathrm{d}\Phi_{N+2}}{\mathrm{d}\Phi_N}\Theta^{\mathrm{PS}}(\Phi_{N+2})\Bigg[\big[RR\;\Theta_{N+1}\big](\Phi_{N+2})\overline{\Theta}^{\mathrm{PS}}_{\mathrm{proj}}(\widetilde{\Phi}_{N+1})+\big[RR\;\Theta_{N+2}\big](\Phi_{N+2})\Bigg]\\
&\quad\times\;\big[\mathcal{O}(\Phi_{N+2})-\mathcal{O}(\Phi_N)\big]\,.
\end{aligned}
$$

It is important to point out that in the equation above there are three different mappings involved: (i) the splitting mapping $\Phi_{N+1}\to\Phi_{N+2}$ used in the NLO calculation, (ii) the projection $\Phi_{N+1}\to\Phi_N$ used by the splitting function in the subtraction counterterm and (iii) the projections $\Phi_{N+1,2}\to\Phi_N$ used in evaluating the observable that act as subtraction according to the P2B method. While there is no constraint for the mapping (i), we have already explained that the projection used in (ii) for the splitting functions is severely constrained to preserve the generation restrictions. Moreover, the last projection (iii) of the P2B method also needs to preserve the generation cuts, such that one can safely write $\Theta^{\mathrm{PS}}(\Phi_{N+2}) = \Theta^{\mathrm{PS}}(\Phi_{N+1}) = \Theta^{\mathrm{PS}}(\Phi_N)$ and derive the formula above. This is the assumption we have relied upon in the derivation of eq. (3.9), which is satisfied by the implementations studied in this paper. A possible alternative is to avoid the usage of generations restrictions altogether and rely instead on a suppression factor that appropriately regulates the divergencies. In this case one can avoid the requirements on the P2B mappings, but the inverse of the suppression factor, which can be a very large number near the IR limits, needs to be included in the event weight, affecting every observable calculated from it. This procedure, while theoretically correct, requires the cancellation between very large numbers and, as such, is more prone to numerical inaccuracies and spikes in the final distributions. The results we obtained during our initial tests of this alternative approach seem to confirm this behaviour.

4 Results and validation

In this section we discuss the numerical implementation, presenting separately our results for the cases of Z boson and Z+jet production at the LHC. We consider the processes

$$
pp\to\gamma^*/Z(\to\ell^+\ell^-)(+\mathrm{jet})+X\,,
$$

at $\sqrt{s}=13\,\mathrm{TeV}$. The results are obtained in the electroweak G_μ-scheme, using a complex mass scheme for the unstable internal particles. We adopted the following values for the input parameters:

$$
\begin{aligned}
m_{\mathrm{Z}} &= 91.1876\,\mathrm{GeV}\,, & \Gamma_{\mathrm{Z}} &= 2.4952\mathrm{GeV}\,,\\
m_{\mathrm{W}} &= 80.379\,\mathrm{GeV}\,, & \Gamma_{\mathrm{W}} &= 2.0850\mathrm{GeV}\,,\\
m_{\mathrm{t}} &= 173.1\,\mathrm{GeV}\,, & G_\mu &= 1.1663787\times10^{-5}\mathrm{GeV}^{-2}\,.
\end{aligned}
$$

JHEP01(2026)065

We use `NNPDF31_nnlo_as_0118` as PDF set [86]. All the matrix elements used in the NLO calculations above $\mathcal{T}_\delta$ are taken from OpenLoops2 [87].

4.1 Results for neutral Drell-Yan production

For the Drell-Yan process, the factorisation and renormalization scales are both set equal to the dilepton invariant mass, $\mu_R = \mu_F = M_{\ell^+\ell^-}$. We impose generation cuts on the invariant mass of the lepton anti-lepton pair such that

$$\Theta^{\text{PS}}(\Phi_0) = \theta\big(50\,\text{GeV} \leq M_{\ell^+\ell^-} \leq 150\,\text{GeV}\big)\,.$$

Since the phase space mappings employed for colour-singlet production processes in Geneva always preserve $M_{\ell^+\ell^-}$, for simplicity, we omit this condition from the formulas, as it factorizes uniformly across all terms.

Given that the NLO results can easily be obtained with a local subtraction and our main goal is to study the precision and numerical accuracy of our approach to calculate the NNLO corrections, in the following we only present results for the most-computationally-demanding pure NNLO correction coefficients. For this reason, we do not include any scale variations, which are only meaningful in the complete NNLO predictions. However, the seven-point independent variations of (μ_R, μ_F) have been validated along with the central predictions that we show in this section. Since the separation between different initial partonic channels does also depend on the factorization scale, we do not present results separated according to the initial state flavours, despite the strong cancellations that there might be between the NNLO corrections to different partonic luminosities.

We focus on the total NNLO coefficient and to highlight the dependence of them on the available phase space we show a limited set of NNLO distributions: $\mathrm{d}\sigma/\mathrm{d}M^2_{\ell^+\ell^-}$, $\mathrm{d}\sigma/\mathrm{d}Y_{\ell^+\ell^-}$, $\mathrm{d}\sigma/\mathrm{d}p_T^{\ell^-}$ and $\mathrm{d}\sigma/\mathrm{d}p_T^{\ell^+}$. For the total NNLO coefficient we also present results obtained in a fiducial region defined by the following ATLAS cuts [88]

$$\begin{aligned} &66\,\text{GeV} \leq M_{\ell^+\ell^-} \leq 116\,\text{GeV}, && |Y_{\ell^-}| \leq 2.5, && |Y_{\ell^+}| \leq 2.5, \\ &p_T^{\ell^-} \geq 27\,\text{GeV}, && p_T^{\ell^+} \geq 27\,\text{GeV}\,. \end{aligned} \tag{4.1}$$

4.1.1 Pure slicing and zero-jettiness subtraction

Starting from the general subtraction formula derived in (3.8), we specify the expression to the case of zero-jettiness $\mathcal{T}_0$, which is a possible resolution variable for the Drell-Yan production process. We employ a dynamical IR cutoff which depends on $M_{\ell^+\ell^-}$ as

$$\mathcal{T}_\delta(M_{\ell^+\ell^-}) = 10^{-4} \cdot M_{\ell^+\ell^-}, \tag{4.2}$$

and, given the restrictions on the generated phase space, implies that $\mathcal{T}_\delta$ varies in the range $5 \cdot 10^{-3}\,\text{GeV} < \mathcal{T}_\delta(M_{\ell^+\ell^-}) < 1.5 \cdot 10^{-2}\,\text{GeV}$. The upper limit where the subtraction is applied, $\mathcal{T}_0^{\text{cut}}(M_{\ell^+\ell^-}) \gg \mathcal{T}_\delta(M_{\ell^+\ell^-})$, is also chosen to be dynamical as

$$\mathcal{T}_0^{\text{cut}}(M_{\ell^+\ell^-}) = 10^{-2} \cdot M_{\ell^+\ell^-}\,, \tag{4.3}$$

JHEP01(2026)065

so that it varies in the range $0.5\,\text{GeV} < \mathcal{T}_0^{\text{cut}}(M_{\ell^+\ell^-}) < 1.5\,\text{GeV}$. We find

$$\begin{aligned}\mathcal{O}_{\delta\text{NNLO}}(\Phi_0) = \frac{\mathrm{d}\Sigma^{\delta\text{NNLO}}_{0,\text{sub.}}}{\mathrm{d}\Phi_0}(\mathcal{T}_0^{\text{cut}}(M_{\ell^+\ell^-}))\,\mathcal{O}(\Phi_0) + \int \frac{\mathrm{d}\Phi_1}{\mathrm{d}\Phi_0}\Big\{\theta(\mathcal{T}_0(\Phi_1) > \mathcal{T}_\delta(M_{\ell^+\ell^-})) \\ \times \Big[RV(\Phi_1)\mathcal{O}(\Phi_1) + \int \frac{\mathrm{d}\Phi_2}{\mathrm{d}\Phi_1}[RR\ \Theta_1](\Phi_2)\mathcal{O}(\Phi_2)\theta(\mathcal{T}_0(\Phi_2) > \mathcal{T}_\delta(M_{\ell^+\ell^-})) \\ - \frac{\mathrm{d}\sigma^{\delta\text{NNLO}}_{0,\text{sub.}}}{\mathrm{d}\Phi_0\mathrm{d}\mathcal{T}_0}\,P(\Phi_1)\mathcal{O}(\Phi_0)\theta(\mathcal{T}_0(\Phi_1) < \mathcal{T}_0^{\text{cut}}(M_{\ell^+\ell^-}))\Big]\Big\} \\ + \int \frac{\mathrm{d}\Phi_2}{\mathrm{d}\Phi_0}\Big[[RR\ \Theta_1](\Phi_2)\theta(\mathcal{T}_0(\widetilde{\Phi}_1) < \mathcal{T}_\delta(M_{\ell^+\ell^-})) + [RR\ \Theta_2](\Phi_2)\Big] \\ \times\ \mathcal{O}(\Phi_2)\,\theta(\mathcal{T}_0(\Phi_2) > \mathcal{T}_\delta(M_{\ell^+\ell^-}))\,.\end{aligned} \tag{4.4}$$

In the formula above, we set

$$\frac{\mathrm{d}\Sigma^{\delta\text{NNLO}}_{0,\text{sub.}}}{\mathrm{d}\Phi_0}(\mathcal{T}_0^{\text{cut}}) = \frac{\mathrm{d}\Sigma^{\text{NNLL}'}_{0}}{\mathrm{d}\Phi_0}(\mathcal{T}_0^{\text{cut}})\Big|_{\mathcal{O}(\alpha_s^2)} \qquad \text{and} \qquad \frac{\mathrm{d}\sigma^{\delta\text{NNLO}}_{0,\text{sub.}}}{\mathrm{d}\Phi_0\mathrm{d}\mathcal{T}_0} = \frac{\mathrm{d}\Sigma^{\text{NNLL}'}_{0}}{\mathrm{d}\Phi_0\mathrm{d}\mathcal{T}_0}\Big|_{\mathcal{O}(\alpha_s^2)}\,, \tag{4.5}$$

where the LP NNLL′ $\mathcal{T}_0$ results for the resummed-expanded cumulant and spectrum[2] on the right hand side were evaluated in refs. [45, 51]. At LP accuracy, it can be shown that the resummed-expanded cumulant and spectrum in $\mathcal{T}_0$ factorize, in the limit $\mathcal{T}_0^{\text{cut}} \ll M_{\ell^+\ell^-}$ or $\mathcal{T}_0 \ll M_{\ell^+\ell^-}$, as a product of a hard function times the convolution of two beam functions and a soft function [89]. In addition, note that in eq. (4.4) there is not an explicit $\overline{\Theta}^{\text{PS}}_{\text{proj}}$ contribution since the generation cuts on $M_{\ell^+\ell^-}$ are always preserved by the mappings. The second to last line is included to add back the points which satisfy the conditions $\theta(\mathcal{T}_0(\Phi_2) > \mathcal{T}_\delta)\,\theta(\mathcal{T}_0(\widetilde{\Phi}_1) < \mathcal{T}_\delta)$ and could not be generated via the FKS $\Phi_1 \to \Phi_2$ splitting, which is employed in this calculation. The splitting functions $P(\Phi_1)$ also utilize a FKS mapping for the $\Phi_1 \to \Phi_0$ projections, hence they also preserve $M_{\ell^+\ell^-}$.

The slicing formula can be easily recovered from eq. (4.4) as a special case by setting $\mathcal{T}_0^{\text{cut}}(M_{\ell^+\ell^-}) = \mathcal{T}_\delta(M_{\ell^+\ell^-})$ as defined in eq. (4.2). From this follows that the cumulant in the first line of eq. (4.4) is evaluated at $\mathcal{T}_\delta(M_{\ell^+\ell^-})$ and the subtraction term in the third line of eq. (4.4) effectively disappear from the equation.

In the first column of table 1 we compare the $\mathcal{O}(\alpha_s^2)$ corrections to the total Drell-Yan cross section coefficients obtained via the pure slicing method and with the nonlocal subtraction. We first notice how these results, summed over all the partonic channels and integrated over the available phase space, result in corrections which are negative and $\leq 1\%$ of the total NLO cross section. We also find that they are consistent within integration errors, and under equivalent conditions of running time and machine type, the numerical integration error of the subtraction method is slightly reduced compared to the pure slicing implementation.

We then present the results for the cross section within the ATLAS fiducial region in the second column. Also in this case we observe a marginal reduction in the error when performing a nonlocal subtraction, despite the final result still being affected by sizable fiducial power corrections (see section 4.1.3).

[2]We remark that the $\mathcal{O}(\alpha_s{}^2)$ expansion of the NNLL′ and the N^{3}LL resummed results are identical for both the cumulant and the spectrum, so we can equivalently use either one. These are also called the singular NNLO cross section cumulant and spectrum, respectively.

JHEP01(2026)065

Method	$\mathcal{O}(\alpha_s{}^2)$ corr. [pb]	$\mathcal{O}(\alpha_s{}^2)$ corr. with ATLAS fid. cuts [pb]
Slicing	-14.45 ± 0.56	-10.13 ± 0.33
Subtraction	-15.03 ± 0.49	-10.61 ± 0.28

Table 1. Comparison of NNLO corrections to the Drell-Yan cross sections between the pure slicing and the nonlocal subtraction implementations. The reported uncertainty refers exclusively to the error from numerical integration.

The comparison of the NNLO differential distributions is instead shown in figure 1, for the invariant mass and rapidity of the dilepton system in the upper panels and for the transverse momentum[3] and rapidity of the negatively charged lepton coming from the Z decay in the lower panels. As for the more inclusive results, we observe a complete agreement and a mild reduction of the statistical uncertainties when performing the nonlocal subtraction.

4.1.2 Adding subleading inclusive power corrections

Our choice of using the LP term in the expansion of the full cross section as $\mathcal{T}_0 \to 0$ when defining the 'subtraction' cross section for $\mathcal{T}_0 \leq \mathcal{T}_\delta$ makes our predictions subject to an error, $\Delta\sigma$, that can be inferred from the corrections that the $\mathcal{T}_0$ factorisation theorem receives and follows a power-like trend $\Delta\sigma \sim \mathcal{O}(\mathcal{T}_\delta/M_{\ell^+\ell^-})$ [90, 91]. This is well appreciated and has been previously investigated in the literature [34, 37, 44], leading to their calculation at NLO [92–94], NNLO [48, 92, 95] and, more recently, at N^{3}LO [96]. In these works, it was shown that despite the overall $\mathcal{T}_0$ power suppression of $\Delta\sigma$, the presence of logarithmic terms on the resolution variable necessitates extremely small values of $\mathcal{T}_\delta$ in order to meet a sensible precision goal in theoretical predictions. In turn, this is a non-trivial requirement for the calculation that involves (at least) one resolved emission, since the corresponding matrix elements have to be evaluated close to the IR-singular limits of QCD. A way to mitigate this issue and systematically improve the subtractions, is to include (some of) these power suppressed terms as part of the 'subtraction' cross section. This allows for higher values of $\mathcal{T}_\delta$ while keeping the same accuracy goal and reducing the numerical integration error or, as a corollary, for an improved accuracy goal while keeping $\mathcal{T}_\delta$ at the same value.

For a practical implementation in GENEVA, the $\mathcal{T}_0$ differential results of ref. [48] for the leading-log (LL) NLP partonic coefficient are included in the subtracted spectrum

$$\frac{\mathrm{d}\sigma^{\delta\mathrm{NNLO}}_{0,\mathrm{sub.}}}{\mathrm{d}\Phi_0 \mathrm{d}\mathcal{T}_0} = \frac{\mathrm{d}\sigma^{\mathrm{NNLL}'}_0}{\mathrm{d}\Phi_0 \mathrm{d}\mathcal{T}_0}\bigg|_{\mathcal{O}(\alpha_s^2)} + \frac{1}{M_{\ell^+\ell^-}} \sum_\kappa \left[C^{(2,2)}_{\kappa,3} \ln^3\left(\frac{\mathcal{T}_0}{M_{\ell^+\ell^-}}\right)\right], \tag{4.6}$$

where we denote the relevant partonic channels by $\kappa = \{q\bar{q}, qg, \ldots\}$ and the LL NLP coefficients $C^{(2,2)}_{\kappa,3}$ are obtained by the partonic ones in eqs. (36) and (37) of ref. [48] after the convolution with the PDFs.

At this point we can distinguish two possible ways of including the NLP corrections in the cumulant. In the first approach, which we refer to as 'spectrum log-counting', we use

[3] The distribution of the transverse momentum of any lepton coming from the Z decay is NNLO only below the Jacobian peak, $p_T^{\ell^\pm} \leq M_{\ell^+\ell^-}/2$, because the double virtual contributions can only be present there.

JHEP01(2026)065

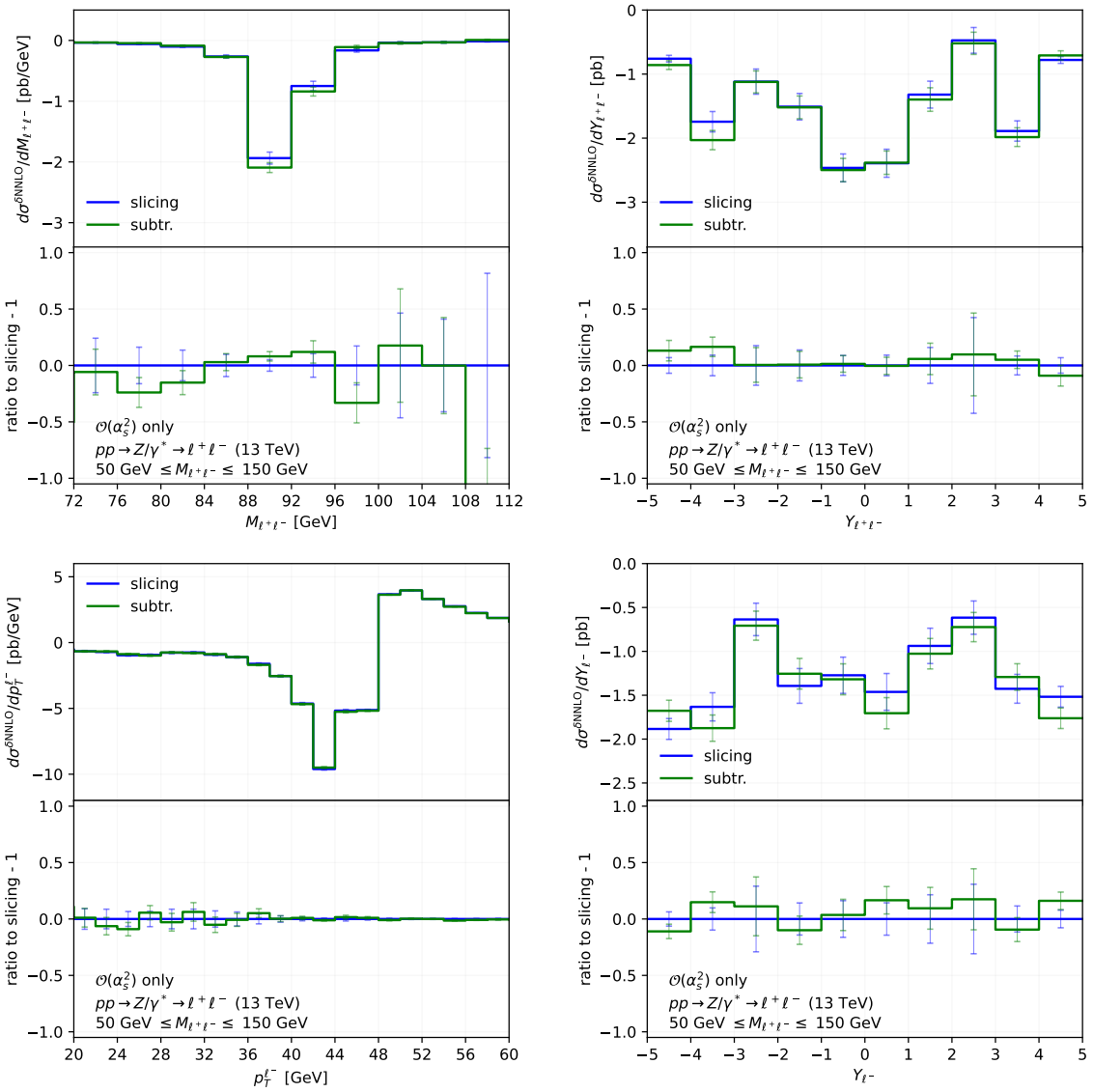

Figure 1. Comparison of the Drell-Yan $\mathcal{O}(\alpha_s{}^2)$ corrections for a set of differential distributions between the slicing and subtraction approaches.

as 'subtraction' term the LP cross section together with the LL NLP coefficients as given in eq. (4.6). After integrating the spectrum of eq. (4.6) up to $\mathcal{T}_0^{\rm cut}$ we get

$$\frac{\mathrm{d}\Sigma_{0,\rm sub.}^{\delta\rm NNLO}}{\mathrm{d}\Phi_0}(\mathcal{T}_0^{\rm cut}) = \frac{\mathrm{d}\Sigma_0^{\rm NNLL'}}{\mathrm{d}\Phi_0}(\mathcal{T}_0^{\rm cut})\bigg|_{\mathcal{O}(\alpha_s^2)} + \frac{\mathcal{T}_0^{\rm cut}}{M_{\ell^+\ell^-}} \sum_\kappa \left[\sum_{m=0}^{3} A_{\kappa,m}^{(2,2)} \ln^m\left(\frac{\mathcal{T}_0^{\rm cut}}{M_{\ell^+\ell^-}}\right)\right], \quad (4.7)$$

with $A_{\kappa,0}^{(2,2)} = -A_{\kappa,1}^{(2,2)} = 2A_{\kappa,2}^{(2,2)} = -6A_{\kappa,3}^{(2,2)} = -6C_{\kappa,3}^{(2,2)}$. In spectrum log-counting all the terms above must be retained such that the dependence on $\mathcal{T}_0^{\rm cut}/M_{\ell^+\ell^-}$ properly cancels between the differential subtraction and the cumulant cross section. In the second approach, which we refer to as 'cumulant log-counting', we perform the differential subtractions between $\mathcal{T}_\delta \leq \mathcal{T}_0 \leq \mathcal{T}_0^{\rm cut}$ using just the LP cross section as 'subtraction' term and only include in the cumulant the highest-power logarithm of eq. (4.7). This practically means that only the

JHEP01(2026)065

Subtraction with	$\mathcal{O}(\alpha_s{}^2)$ corr. [pb]	$\mathcal{O}(\alpha_s{}^2)$ corr. with ATLAS fid. cuts [pb]
spectrum log-counting	-13.64 ± 0.36	-10.11 ± 0.20
cumulant log-counting	-14.66 ± 0.51	-10.41 ± 0.29
NNLOJET	-13.40 ± 0.01	-1.63 ± 0.35

Table 2. Comparison of the Drell-Yan $\mathcal{O}(\alpha_s{}^2)$ total cross section coefficient using two different approaches for the inclusion of LL NLP inclusive power corrections. The reported uncertainty refers exclusively to the error from numerical integration.

$\mathcal{T}_\delta = \mathcal{T}_0^{\text{cut}}$	LL NLP Cum. [pb]	LL NLP Spect. [pb]	$\mathcal{O}(\alpha_s^2)$ no NLP [pb]
$M_{\ell\ell}$	0 ± 0	-106.47 ± 0.065	52.907 ± 0.007
$10^{-1} \times M_{\ell\ell}$	-21.66 ± 0.01	-85.06 ± 0.05	46.7 ± 0.1
$10^{-2} \times M_{\ell\ell}$	-17.33 ± 0.01	-34.59 ± 0.021	14.44 ± 0.39
$10^{-3} \times M_{\ell\ell}$	-5.849 ± 0.004	-9.232 ± 0.006	-4.4 ± 1
$10^{-4} \times M_{\ell\ell}$	-1.3865 ± 0.0008	-1.947 ± 0.001	-14.45 ± 0.56

Table 3. Comparison of the Drell-Yan $\mathcal{O}(\alpha_s{}^2)$ NLP corrections in the two logarithmic counting schemes as a function of the slicing parameter. The reported uncertainty refers exclusively to the error from numerical integration.

term proportional to $A_{\kappa,3}^{(2,2)}$ is taken into account whereas $A_{\kappa,m}^{(2,2)}$, $m = 0, 1, 2$ are neglected. This choice, albeit unfounded as it may be regarded, is no more arbitrary than keeping all terms in eq. (4.7) because they are anyway only obtained by the integration of the LL NLP coefficient and therefore they are missing contributions from the subleading logarithmic NLP terms in the spectrum. For this reason, it is not clear *a priori* whether including (or not) the $A_{\kappa,m}^{(2,2)}$, $m = 0, 1, 2$ terms only coming from the integration of the LL NLP spectrum coefficient does improve the theoretical predictions.[4] Despite the cumulant log-counting might seem the safest choice, due to the fact that the highest logarithm does not receive contributions from the integration of unknown subleading logarithmic NLP terms, one should still be careful because only including the $A_{\kappa,3}^{(2,2)}$ term can miss sizable numerical cancellations with the unknown NLP subleading logarithmic terms. Therefore, we investigate both possibilities, in order to have a rough estimate on the size of the cancellations between the integral of NLP logarithmic terms.

In table 2 we compare the $\mathcal{O}(\alpha_s^2)$ corrections to the total rates, obtained with the cumulant and spectrum logarithmic countings, for both inclusive and fiducial phase space regions. We find again that these results are consistent within integration errors, and under equivalent conditions of running time and machine type. The numerical integration errors are also similar, although the results obtained with the spectrum log-counting looks marginally better. This is a consequence of including the LL NLP terms in the subtraction of the spectrum. In any case, we observe that for the small choice of the IR cutoff $\mathcal{T}_\delta$ used for these predictions,

[4] As far as we understand, the cumulant log-counting in a pure slicing calculation is the choice adopted by MCFM in refs. [37, 97].

JHEP01(2026)065

the effect of including the LL NLP corrections for both logarithmic countings is anyway rather small. In the last row of the table, we report the corresponding predictions from NNLOJET. We start by noticing how the local NNLO subtraction in NNLOJET is particularly efficient in the predictions of the inclusive corrections. This is a peculiarity of applying the antenna subtraction to the Drell-Yan process, where the subtraction term is very similar to the Drell-Yan matrix element. Already looking at the corrections in the fiducial regions we see how the statistical errors increase. Our results for the corrections in the ATLAS fiducial region are instead in disagreement with NNLOJET. This is expected since this observable is indeed strongly sensitive to FPCs which are not yet included in the results of table 2.

In order to investigate the genuine size of NLP corrections, we present in table 3 the $\mathcal{O}(\alpha_s^2)$ LL NLP corrections to the cumulant obtained in the two logarithmic counting schemes for different values of the slicing parameter. For comparison, we also include a third column where we present the $\mathcal{O}(\alpha_s^2)$ corrections obtained with the slicing implementation excluding NLP corrections and using the corresponding value of the slicing parameter reported on the first column.[5] The LL NLP corrections have the expected behaviour, they decrease when the cutoff is decreasing. For values of the cutoff $\mathcal{T}_\delta = \mathcal{T}_0^{\text{cut}} \in [10^{-1}, 10^{-3}]\, M_{\ell\ell}$, the LL NLP corrections are large and, in particular, at the cutoff value $\mathcal{T}_\delta = \mathcal{T}_0^{\text{cut}} = 10^{-3}\, M_{\ell\ell}$ they account for more than 100% of the total correction obtained with the same slicing cutoff value. They become approximately one order of magnitude smaller than the total NNLO correction only starting at $\mathcal{T}_\delta = \mathcal{T}_0^{\text{cut}} = 10^{-4}\, M_{\ell\ell}$. We also notice that spectrum log-counting results are larger in absolute value than the corresponding cumulant log-counting results. In particular, we would like to point out that while for $\mathcal{T}_\delta = \mathcal{T}_0^{\text{cut}} = M_{\ell\ell}$ the cumulant log-counting result correctly vanishes, the spectrum log-counting result does not vanish due to the presence of non-logarithmic terms.

The NLP results presented in this table should be interpreted with caution, as only the LL contribution is currently fully known. It remains possible that the currently unknown subleading logarithmic terms (NLL and beyond) could contribute with an opposite sign with respect to the LL contribution, potentially reducing the overall impact of NLP corrections.

In figure 2 we show predictions for the $\mathcal{O}({\alpha_s}^2)$ coefficient of a set of differential distributions for the two LL NLP counting schemes and we find very good agreement between them. Similarly to the total cross section coefficients, we also notice that the results obtained with the spectrum counting scheme show smaller statistical integration errors across all distributions. The statistical integration error of NNLOJET is very small for the $M_{\ell^+\ell^-}$ and $Y_{\ell^+\ell^-}$ inclusive distributions while it sensibly increases for $p_T^{\ell^-}$ and Y_{ℓ^-}. As explained above, this is a feature of the local antenna subtraction method for this particular process. The agreement with NNLOJET is also very good and we observe an expected difference with our calculations for the $p_T^{\ell^-}$ distribution in the region $44\,\text{GeV} \leq p_T^{\ell^-} \leq 48\,\text{GeV}$. Also this observable is indeed very sensitive to FPCs, which are not yet included in our predictions. This plot highlights the importance of their inclusion, which will be discussed in the next section (compare for example to the corresponding plot in figure 3). One however should always keep in mind that

[5] We note that the numerical integration errors reported in the last column of table 3 for values of $\mathcal{T}_\delta = \mathcal{T}_0^{\text{cut}} > 10^{-4}\, M_{\ell\ell}$ are obtained with shorter dedicated runs compared to the very last entry which is instead taken from table 1. This explains why the last error is smaller then the one with the larger cutoff.

JHEP01(2026)065

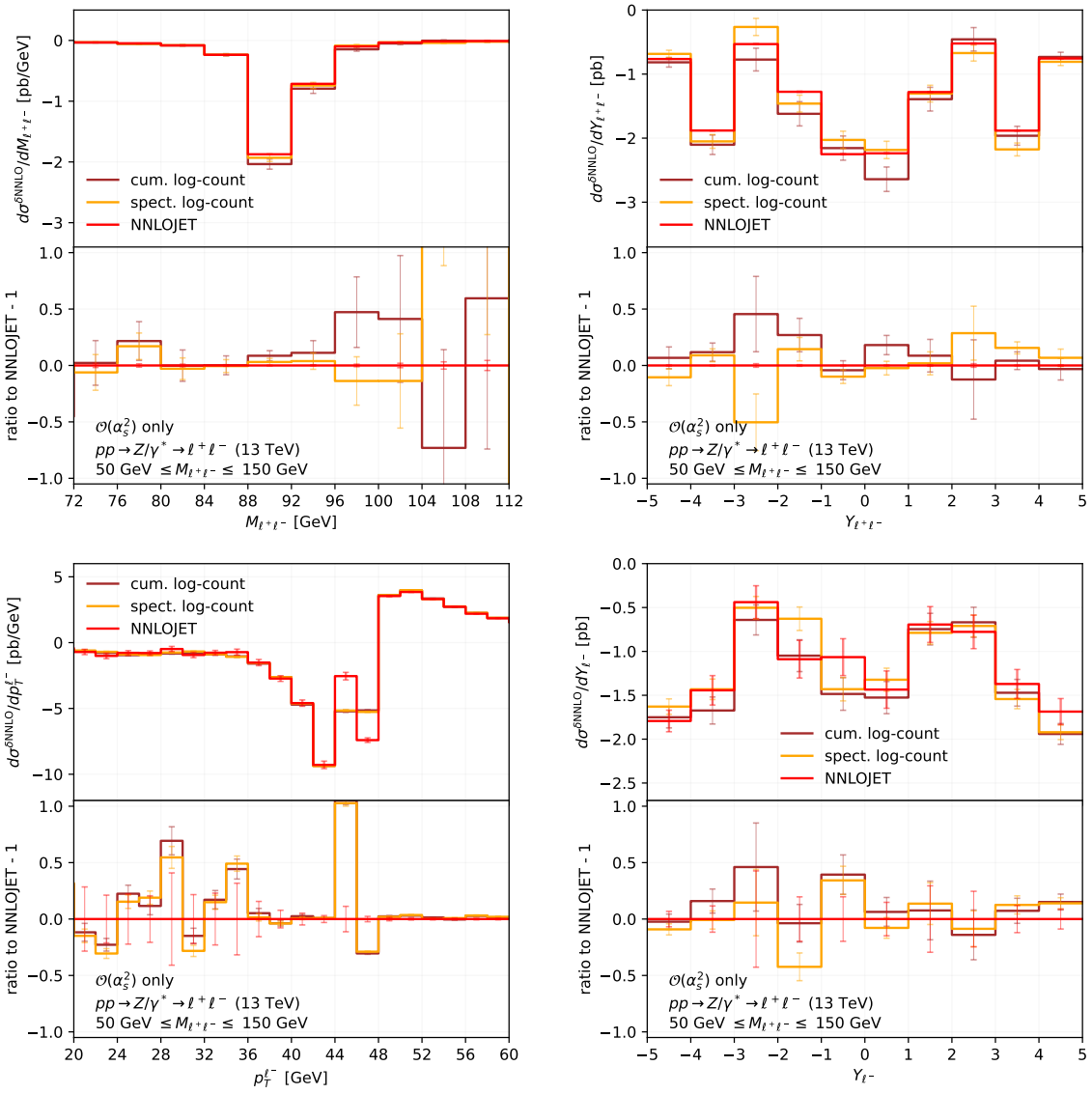

Figure 2. Comparison of the Drell-Yan $\mathcal{O}(\alpha_s{}^2)$ corrections for a set of differential distributions between NNLOJET and the two LL NLP counting schemes implementations.

any fixed-order prediction is intrinsically problematic in describing the region close to the Jacobian peak, $M_{\ell^+\ell^-}/2$, for this distribution, because Sudakov-shoulder logarithms become important and only after their resummation one obtains physically-sensible results [43, 98, 99].

4.1.3 Inclusion of FPC corrections

Lastly, we include the fiducial power corrections, specifying eq. (3.9) for zero-jettiness subtraction and using the FKS mapping recursively for the $\Phi_2 \to \Phi_1 \to \Phi_0$ projections which are needed for the evaluation of the subtracted observable according to the P2B method.

JHEP01(2026)065

Subtraction with FPC and	$\mathcal{O}(\alpha_s{}^2)$ corr. [pb]	$\mathcal{O}(\alpha_s{}^2)$ corr. with ATLAS fid. cuts [pb]
spectrum log-counting	-13.85 ± 0.32	-1.14 ± 0.18
cumulant log-counting	-13.21 ± 0.33	-0.84 ± 0.19
NNLOJET	-13.40 ± 0.01	-1.63 ± 0.35

Table 4. Comparison with NNLOJET of the Drell-Yan $\mathcal{O}(\alpha_s{}^2)$ total cross section coefficient after including FPC corrections using the two different approaches for the inclusion of LL NLP inclusive power corrections in GENEVA. The reported uncertainty refers exclusively to the error from numerical integration.

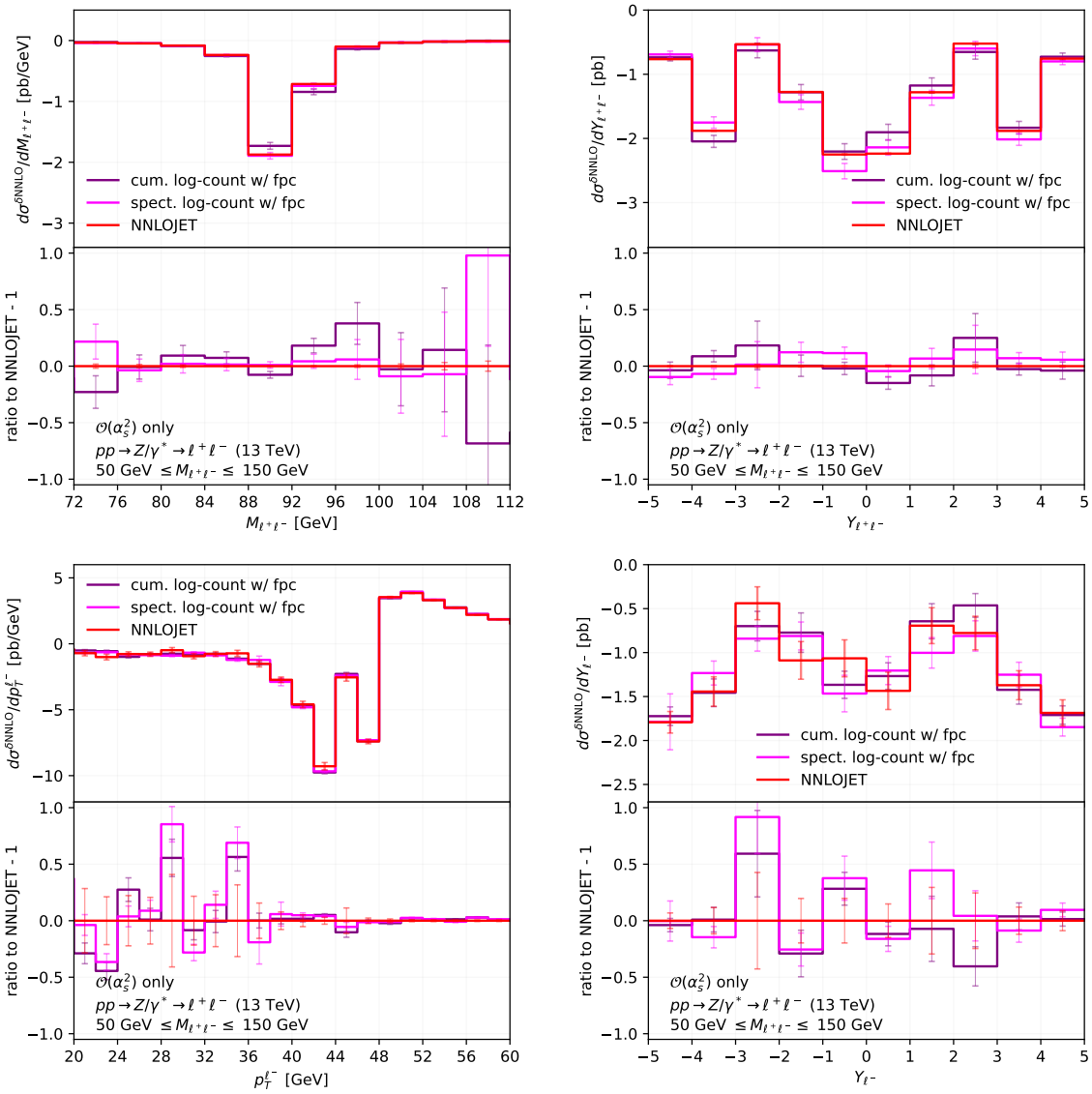

Figure 3. Comparison of the Drell-Yan $\mathcal{O}(\alpha_s{}^2)$ corrections for a set of differential distributions between NNLOJET and the two LL NLP counting schemes implementations with the inclusion of FPCs.

JHEP01(2026)065

We find

$$\begin{aligned}\mathcal{O}_{\delta\mathrm{NNLO}}(\Phi_0) = \Bigg\{ & \frac{\mathrm{d}\Sigma^{\delta\mathrm{NNLO}}_{0,\mathrm{sub.}}}{\mathrm{d}\Phi_0}(\mathcal{T}_0^{\mathrm{cut}}(M_{\ell^+\ell^-})) + \int \frac{\mathrm{d}\Phi_1}{\mathrm{d}\Phi_0}\Big\{\theta(\mathcal{T}_0(\Phi_1) > \mathcal{T}_\delta(M_{\ell^+\ell^-})) \\ & \times \Big[RV(\Phi_1) + \int \frac{\mathrm{d}\Phi_2}{\mathrm{d}\Phi_1}[RR\ \Theta_1](\Phi_2)\theta(\mathcal{T}_0(\Phi_2) > \mathcal{T}_\delta(M_{\ell^+\ell^-})) \\ & - \frac{\mathrm{d}\sigma^{\delta\mathrm{NNLO}}_{0,\mathrm{sub.}}}{\mathrm{d}\Phi_0\mathrm{d}\mathcal{T}_0}\ P(\Phi_1)\theta(\mathcal{T}_0(\Phi_1) < \mathcal{T}_0^{\mathrm{cut}}(M_{\ell^+\ell^-}))\Big]\Big\} \\ & + \int \frac{\mathrm{d}\Phi_2}{\mathrm{d}\Phi_0}\Big[[RR\ \Theta_1](\Phi_2)\theta(\mathcal{T}_0(\widetilde{\Phi}_1) < \mathcal{T}_\delta(M_{\ell^+\ell^-})) \\ & + [RR\ \Theta_2](\Phi_2)\Big]\theta(\mathcal{T}_0(\Phi_2) > \mathcal{T}_\delta(M_{\ell^+\ell^-}))\ \Big\}\mathcal{O}(\Phi_0) \\ & + \int \frac{\mathrm{d}\Phi_1}{\mathrm{d}\Phi_0}\Big[RV(\Phi_1)[\mathcal{O}(\Phi_1)-\mathcal{O}(\Phi_0)] + \int \frac{\mathrm{d}\Phi_2}{\mathrm{d}\Phi_1}[RR\ \Theta_1](\Phi_2)[\mathcal{O}(\Phi_2)-\mathcal{O}(\Phi_0)]\Big] \\ & + \int \frac{\mathrm{d}\Phi_2}{\mathrm{d}\Phi_0}\Big[[RR\ \Theta_2](\Phi_2)[\mathcal{O}(\Phi_2)-\mathcal{O}(\Phi_0)]\Big]\,. \end{aligned} \tag{4.8}$$

In table 4 we compare the $\mathcal{O}(\alpha_s^2)$ corrections to the total production cross section corrections obtained with the cumulant and spectrum logarithmic countings, also including FPCs, for both inclusive and fiducial phase space regions. The central values for the inclusive corrections are not sensitive to the inclusion of FPCs and indeed they are compatible with the results shown in table 2. The inclusion of FPCs has instead a fundamental impact on the fiducial cross sections results computed using both counting schemes: it reduces the size of $\mathcal{O}(\alpha_s^2)$ corrections giving compatible results. Given the larger uncertainty reported by NNLOJET for this quantity, all these predictions are in agreement, resolving the tension found in table 2.

In figure 3 we show predictions for the $\mathcal{O}({\alpha_s}^2)$ coefficient of a set of differential distributions including FPCs. Overall, we observe the same behaviour as in figure 2 for more inclusive quantities, with the notable exception of the $p_T^{\ell^-}$ around the Jacobian peak, which is now in complete agreement with NNLOJET. This is an indication that our implementation correctly captures the fiducial effects.

4.2 Results for neutral Drell-Yan plus one jet production

Moving on to the more complicated case with an extra jet, we now consider the process

$$pp \to \gamma^*/Z(\to \ell^+\ell^-) + \mathrm{jet} + X\,.$$

As for the Drell-Yan case presented in section 4.1, we present results only for the pure NNLO coefficients, which means that all the results presented in this section are at absolute $\mathcal{O}({\alpha_s}^3)$. We do not separate the results according to the initial state flavours neither we include any scale variation, which can only be correctly accounted for in the complete NNLO predictions.

The presence of one jet already at the leading order requires the introduction of a *defining cut* in order to avoid a divergent cross-section. Several choices are possible, as long as the IR region when the jet becomes soft and/or collinear to the beam is avoided. For the

JHEP01(2026)065

present study we have limited ourselves to cutting on zero-jettiness, $\mathcal{T}_0$ or on the transverse momentum q_T of the Z boson. Both quantities vanish when there are no QCD emissions, making them suitable defining cuts, but, due to its vectorial nature, q_T can be zero even in the presence of two back-to-back jets, irrespective of their energy. Because of this property, the phase space regions carved out by cutting on $\mathcal{T}_0$ or q_T are intrinsically different, which gives us a good handle on exploring the dependence of our results on the defining cuts.

We therefore show results for the $\mathcal{O}({\alpha_s}^3)$ cross section corrections, employing different sets of measurement cuts $\sigma^{\delta\text{NNLO}}(\mathcal{T}_0 > w)$ and $\sigma^{\delta\text{NNLO}}(q_T > w)$ for $w = 1, 10, 50$ and $100\,\text{GeV}$. Similarly, we only focus on a limited set of NNLO differential distributions, namely the zero-jettiness $\mathrm{d}\sigma/\mathrm{d}\mathcal{T}_0$ and the transverse momentum $\mathrm{d}\sigma/\mathrm{d}q_T$ distributions, as well as some distributions of the leptonic decay products of the vector boson with a cut on $\mathcal{T}_0$ or q_T.

At variance with the Drell-Yan production case, now there are potentially more hard scales present in this process. A suitable choice for the factorisation and renormalization scales is

$$\mu_R = \mu_F = \mu_{\text{FO}} = m_T \equiv \sqrt{M^2_{\ell^+\ell^-} + q_T^2}\,, \tag{4.9}$$

where $M_{\ell^+\ell^-}$ is the invariant mass and q_T is the transverse momentum of the colour-singlet system. This variable indeed captures the dynamic of the recoil against a hard jet while providing a nonzero value even when the QCD emissions become soft or collinear. In general however, any choice of a single scale in a multi-scale problem will inevitably generate potentially large logarithms of different scale ratios. When deciding the value for the IR resolution cutoff $\mathcal{T}_\delta$ adopted in the calculation we have to factor in this consideration. We will choose a dynamical cut that balances the accuracy of the calculation by limiting the potentially large scale ratios while, at the same time, avoid a resolution cut too small which will result in an unstable cancellation between terms that are numerically large.

4.2.1 Slicing vs. subtraction

We first implement a simpler slicing approach, using the absolute $\mathcal{O}({\alpha_s}^3)$ contribution of the leading-power singular N^{3}LL $\mathcal{T}_1$ resummed-expanded cumulant calculated in ref. [47] as $\mathrm{d}\Sigma^{\delta\text{NNLO}}_{1,\text{sub.}}/\mathrm{d}\Phi_1$. In order to regulate the divergencies present at Born level, we impose the generation cuts

$$\Theta^{\text{PS}}(\Phi_M) = \theta\big(q_T(\Phi_M) > 10^{-3}\ \text{GeV}\big)\,, \tag{4.10}$$

with q_T the vector boson transverse momentum. We also use a dynamical cut

$$\mathcal{T}_\delta(\Phi_M) = \min\left\{\mathcal{T}_0(\Phi_M)/2, f\big(q_T(\Phi_M)\big)\right\}\,, \tag{4.11}$$

such that the kinematical limit $\mathcal{T}_1(\Phi_2) < \mathcal{T}_0(\Phi_2)/2$ is automatically enforced and the logistic function $f(x)$, defined as

$$f(x) = 10^{-4}\cdot\left(1 + 10^{-2+4/(1+\exp(-0.3x))^5}\right)\,, \tag{4.12}$$

interpolates the effective $\mathcal{T}_\delta$ cutoff between $10^{-4} \leq \mathcal{T}_\delta \leq 10^{-2}$ for $5\,\text{GeV} \lesssim q_T \lesssim 25\,\text{GeV}$. In this way $\mathcal{T}_\delta(\Phi_M)$ captures the multi-scales dynamics in terms of a single, but kinematic-

JHEP01(2026)065

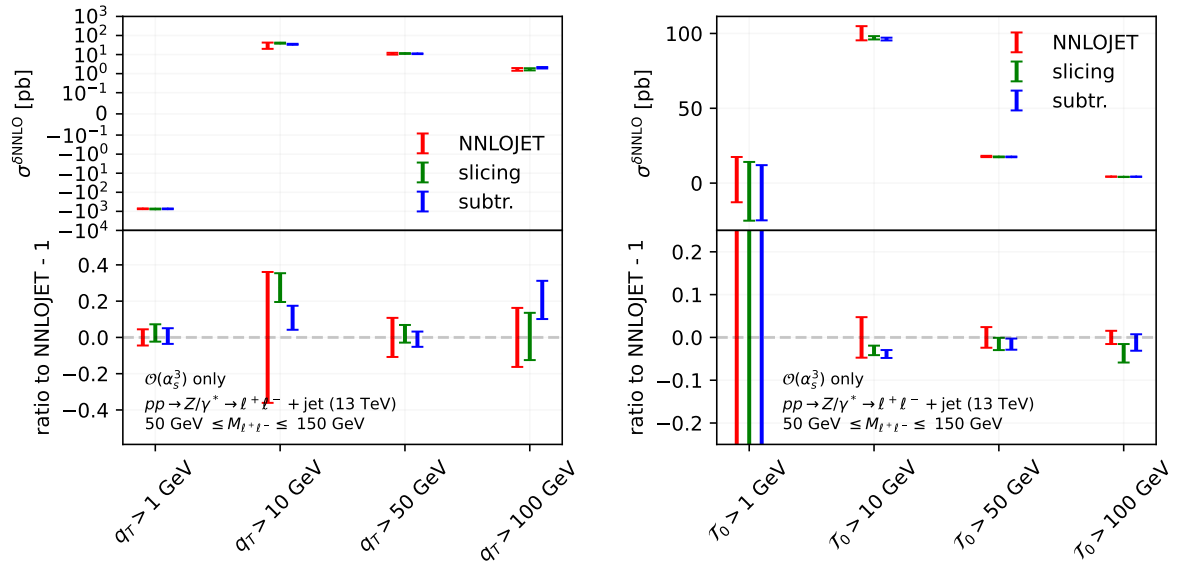

Figure 4. Comparison of the Z+jet $\mathcal{O}({\alpha_s}^3)$ integrated corrections between the slicing and subtraction implementations for different values of the defining cut on q_T (left) and $\mathcal{T}_0$ (right).

dependent, resolution parameter. We therefore arrive at

$$\begin{aligned}\mathcal{O}_{\delta\text{NNLO}}(\Phi_1) = {} & \frac{\mathrm{d}\Sigma_1^{\mathrm{N^3LL}}}{\mathrm{d}\Phi_1}(\mathcal{T}_\delta(\Phi_1))\bigg|_{{\alpha_s}^3} \Theta^{\mathrm{PS}}(\Phi_1)\,\mathcal{O}(\Phi_1) \\ & + \int \frac{\mathrm{d}\Phi_2}{\mathrm{d}\Phi_1}\Big\{ \Theta^{\mathrm{PS}}(\Phi_2)\,\theta(\mathcal{T}_1(\Phi_2) > \mathcal{T}_\delta(\Phi_2))\Big[RV(\Phi_2)\mathcal{O}(\Phi_2) \\ & \quad + \int \frac{\mathrm{d}\Phi_3}{\mathrm{d}\Phi_2}\big[RR\,\Theta_2\,\Theta^{\mathrm{PS}}\big](\Phi_3)\mathcal{O}(\Phi_3)\theta(\mathcal{T}_1(\Phi_3) > \mathcal{T}_\delta(\Phi_3))\Big]\Big\} \\ & + \int \frac{\mathrm{d}\Phi_3}{\mathrm{d}\Phi_1}\Big[\big[RR\,\Theta_2\,\Theta^{\mathrm{PS}}\big](\Phi_3)\Big(\overline{\Theta}^{\mathrm{PS}}_{\mathrm{proj}}(\widetilde{\Phi}_2) + \theta(\mathcal{T}_1(\widetilde{\Phi}_2) < \mathcal{T}_\delta(\widetilde{\Phi}_2))\Big) \\ & \quad + \big[RR\,\Theta_3\,\Theta^{\mathrm{PS}}\big](\Phi_3)\Big]\,\mathcal{O}(\Phi_3)\theta(\mathcal{T}_1(\Phi_3) > \mathcal{T}_\delta(\Phi_3))\,. \end{aligned} \tag{4.13}$$

Since we choose to perform the $\Phi_2 \to \Phi_3$ splitting in the third line using an FKS mapping that does not preserve neither $\mathcal{T}_0$ nor q_T, in the second but last line of the formula above we have to include the $\overline{\Theta}^{\mathrm{PS}}_{\mathrm{proj}}(\widetilde{\Phi}_2) = \theta(q_T(\widetilde{\Phi}_2) < 10^{-3}\ \mathrm{GeV})$ (i.e. the complement of eq. (4.10)) and the $\theta(\mathcal{T}_1(\widetilde{\Phi}_2) < \mathcal{T}_\delta(\Phi_2))$ contributions, that exactly accounts for this mismatch.

In the next step we have extended eq. (4.13) to include a nonlocal subtraction. The subtraction term can again be retrieved as the leading-power $\mathrm{N^3LL}$ $\mathcal{T}_1$ resummed-expanded spectrum from ref. [47]. As explained in section 3.2, the splitting function $P(\Phi_2)$ and the associated mappings are required to preserve both the q_T-defining phase space restriction and the $\mathcal{T}_0$ entering the dynamic cut. We therefore choose to use the $(\mathcal{T}_0, q_T)$-preserving mapping first implemented in GENEVA in ref. [51]. Similarly as for $\mathcal{T}_\delta$, also $\mathcal{T}_1^{\mathrm{cut}}$ is now promoted to be a dynamical cut by

$$\mathcal{T}_1^{\mathrm{cut}}(\Phi_M) = \min\Big\{\mathcal{T}_0(\Phi_M)/2, 10^2 \cdot f(q_T(\Phi_M))\Big\}\,. \tag{4.14}$$

JHEP01(2026)065

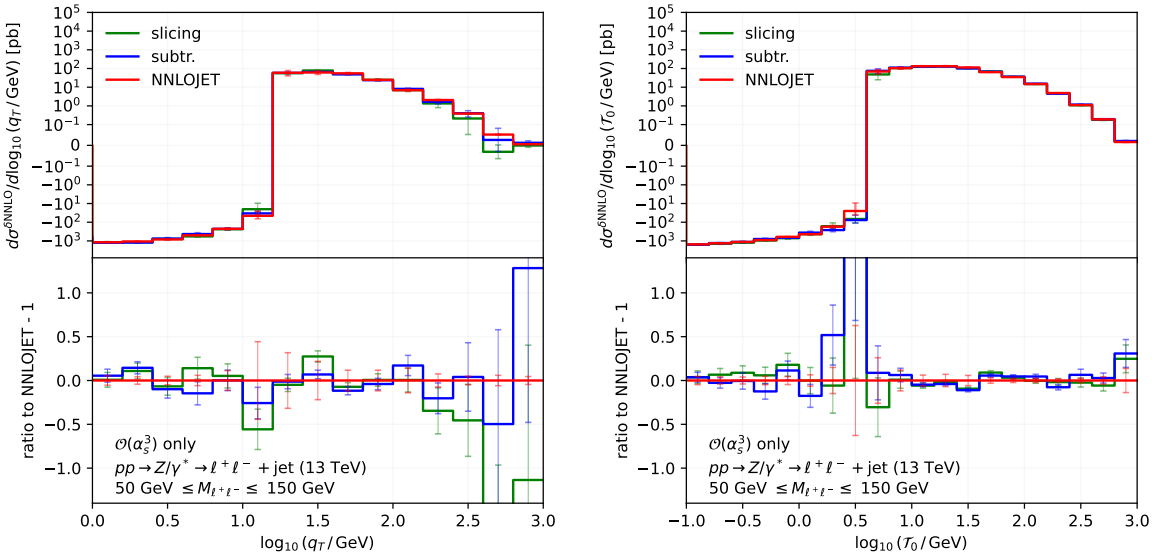

Figure 5. Comparison of the Z+jet $\mathcal{O}({\alpha_s}^3)$ corrections for the q_T (left) and $\mathcal{T}_0$ (right) differential distributions between the slicing and subtraction implementations.

With these choices, we get the formula for the NNLO corrections with a nonlocal subtraction as

$$
\begin{aligned}
\mathcal{O}_{\delta\text{NNLO}}(\Phi_1) = {} & \frac{\mathrm{d}\Sigma_1^{\text{N}^3\text{LL}}}{\mathrm{d}\Phi_1}(\mathcal{T}_1^{\text{cut}}(\Phi_1))\bigg|_{{\alpha_s}^3} \Theta^{\text{PS}}(\Phi_1)\,\mathcal{O}(\Phi_1) \\
& + \int \frac{\mathrm{d}\Phi_2}{\mathrm{d}\Phi_1}\Big\{\Theta^{\text{PS}}(\Phi_2)\theta(\mathcal{T}_1(\Phi_2) > \mathcal{T}_\delta(\Phi_2))\Big[RV(\Phi_2)\mathcal{O}(\Phi_2) \\
& \quad + \int \frac{\mathrm{d}\Phi_3}{\mathrm{d}\Phi_2}\big[RR\,\Theta_2\,\Theta^{\text{PS}}\big](\Phi_3)\mathcal{O}(\Phi_3)\theta(\mathcal{T}_1(\Phi_3) > \mathcal{T}_\delta(\Phi_3)) \\
& \quad - \frac{\mathrm{d}\sigma_1^{\text{N}^3\text{LL}}}{\mathrm{d}\Phi_1\mathrm{d}\mathcal{T}_1}\bigg|_{{\alpha_s}^3} P(\Phi_2)\mathcal{O}(\Phi_1)\theta(\mathcal{T}_1(\Phi_2) < \mathcal{T}_1^{\text{cut}}(\Phi_2))\Big]\Big\} \\
& + \int \frac{\mathrm{d}\Phi_3}{\mathrm{d}\Phi_1}\Big[\big[RR\,\Theta_2\,\Theta^{\text{PS}}\big](\Phi_3)\Big(\overline{\Theta}^{\text{PS}}_{\text{proj}}(\widetilde{\Phi}_2) + \theta(\mathcal{T}_1(\widetilde{\Phi}_2) < \mathcal{T}_\delta(\widetilde{\Phi}_2))\Big) \\
& \quad + \big[RR\,\Theta_3\,\Theta^{\text{PS}}\big](\Phi_3)\Big]\,\mathcal{O}(\Phi_3)\theta(\mathcal{T}_1(\Phi_3) > \mathcal{T}_\delta(\Phi_3))\,.
\end{aligned}
\tag{4.15}
$$

It must be pointed out, however, that in the region where $\mathcal{T}_0(\Phi_M) \leq 2f(q_T(\Phi_M))$ the nonlocal subtraction calculation becomes a pure slicing one, because $\mathcal{T}_1^{\text{cut}} = \mathcal{T}_\delta = \mathcal{T}_0(\Phi_M)/2$.

In figure 4 we compare the results of the slicing and subtraction approaches described above with NNLOJET for the $\mathcal{O}({\alpha_s}^3)$ contributions to the cross sections with different defining cuts in q_T and $\mathcal{T}_0$. We observe good agreement for all values of the cuts, with the results of the subtraction approach giving statistical errors consistently smaller than the corresponding ones obtained with the slicing approach.

In a similar fashion, we compare the q_T and $\mathcal{T}_0$ distributions in figure 5. We observe a similar good agreement with NNLOJET over several orders of magnitude, for both the slicing and subtraction approaches. The statistical errors are now more challenging, for both GENEVA and NNLOJET, especially where the distribution changes sign.

JHEP01(2026)065

4.2.2 Inclusion of FPC corrections

In order to include the fiducial power corrections below the IR cutoff, we can specify the general eq. (3.9) to the one-jettiness case, obtaining

$$
\begin{aligned}
\mathcal{O}_{\delta\mathrm{NNLO}}(\Phi_1) = \Bigg\{ & \frac{\mathrm{d}\Sigma_1^{\mathrm{N^3LL}}}{\mathrm{d}\Phi_1}(\mathcal{T}_1^{\mathrm{cut}}(\Phi_1))\bigg|_{{\alpha_s}^3} \Theta^{\mathrm{PS}}(\Phi_1) \\
& + \int \frac{\mathrm{d}\Phi_2}{\mathrm{d}\Phi_1}\Bigg\{\Theta^{\mathrm{PS}}(\Phi_2)\theta(\mathcal{T}_1(\Phi_2) > \mathcal{T}_\delta(\Phi_2))\Bigg[RV(\Phi_2) \\
& \quad + \int \frac{\mathrm{d}\Phi_3}{\mathrm{d}\Phi_2}\left[RR\ \Theta_2\Theta^{\mathrm{PS}}\right](\Phi_3)\theta(\mathcal{T}_1(\Phi_3) > \mathcal{T}_\delta(\Phi_3)) \\
& \quad - \frac{\mathrm{d}\sigma_1^{\mathrm{N^3LL}}}{\mathrm{d}\Phi_1\mathrm{d}\mathcal{T}_1}\bigg|_{{\alpha_s}^3} P(\Phi_2)\theta(\mathcal{T}_1(\Phi_2) < \mathcal{T}_1^{\mathrm{cut}}(\Phi_2))\Bigg]\Bigg\} \\
& + \int \frac{\mathrm{d}\Phi_3}{\mathrm{d}\Phi_1}\Bigg[\left[RR\ \Theta_2\Theta^{\mathrm{PS}}\right](\Phi_3)\Big(\overline{\Theta}^{\mathrm{PS}}_{\mathrm{proj}}(\widetilde{\Phi}_2) + \theta(\mathcal{T}_1(\widetilde{\Phi}_2) < \mathcal{T}_\delta(\widetilde{\Phi}_2))\Big) \\
& \quad + \left[RR\ \Theta_3\Theta^{\mathrm{PS}}\right](\Phi_3)\Bigg]\theta(\mathcal{T}_1(\Phi_3) > \mathcal{T}_\delta(\Phi_3))\Bigg\}\ \mathcal{O}(\Phi_1) \\
& + \int \frac{\mathrm{d}\Phi_2}{\mathrm{d}\Phi_1}\Theta^{\mathrm{PS}}(\Phi_2)\Bigg[RV(\Phi_2)\left[\mathcal{O}(\Phi_2)-\mathcal{O}(\Phi_1)\right] \\
& \quad + \int \frac{\mathrm{d}\Phi_3}{\mathrm{d}\Phi_2}\left[RR\ \Theta_2\Theta^{\mathrm{PS}}\right](\Phi_3)\left[\mathcal{O}(\Phi_3)-\mathcal{O}(\Phi_1)\right]\Bigg] \\
& \quad + \int \frac{\mathrm{d}\Phi_3}{\mathrm{d}\Phi_1}\Theta^{\mathrm{PS}}(\Phi_3)\Bigg[\left[RR\ \Theta_2\right](\Phi_3)\overline{\Theta}^{\mathrm{PS}}_{\mathrm{proj}}(\widetilde{\Phi}_2) + \left[RR\ \Theta_3\right](\Phi_3)\Bigg]\left[\mathcal{O}(\Phi_3)-\mathcal{O}(\Phi_1)\right].
\end{aligned}
\tag{4.16}
$$

As discussed after eq. (3.9), the formula above is only correct assuming the $\Phi_3 \to \Phi_2 \to \Phi_1$ projections, which are needed for the evaluation of the subtracted observable according to the P2B method, are performed with a mapping that preserves the phase space restrictions at the generation level, i.e. $\Theta^{\mathrm{PS}}(\Phi_3) = \Theta^{\mathrm{PS}}(\Phi_2) = \Theta^{\mathrm{PS}}(\Phi_1) = \theta(q_T(\Phi_M) > 10^{-3}\ \mathrm{GeV})$. This is a very nontrivial requirement that forced us to design a new q_T-preserving mapping, which is applied recursively.

P2B mapping. We first find the closest partons comparing an invariant mass metric for final-state distances and the transverse momentum squared with respect to the beam for the initial-state distances, dubbing them emitted and sister. In the case of a final-state clustering, the spatial three-vector momenta of the closest partons are summed together and the energy of the clustered parton is set equal to the modulus of this sum, thus replacing two massless partons with a new massless one, which is dubbed the mother. All the other final-state partons and colour-neutral objects are left unchanged. In formulae

$$
\tilde{p}_i = p_i \quad \text{for } i \neq \text{emi.}, \text{sis.} \qquad \text{and} \qquad \tilde{p}_{\mathrm{mum}} = (|\vec{p}_{\mathrm{emi.}} + \vec{p}_{\mathrm{sis.}}|, \vec{p}_{\mathrm{emi.}} + \vec{p}_{\mathrm{sis.}})\ .
$$

This implies that the total energy and rapidity of the event are modified because, calling the sum of the four-momenta in the final state before and after the clustering as

$$
p_{\mathrm{fin.}} = \sum_{i\in\text{fin. state}} p_i \qquad \text{and} \qquad \tilde{p}_{\mathrm{fin.}} = \sum_{i\in\text{fin. state}} \tilde{p}_i\,, \quad \text{respectively,}
$$

JHEP01(2026)065

we observe that $\tilde{s} = \tilde{p}^2_{\text{fin.}} \neq p^2_{\text{fin.}}$ and $\tilde{Y} = \frac{1}{2}\log\left(\frac{\tilde{p}^0_{\text{fin.}}+\tilde{p}^z_{\text{fin.}}}{\tilde{p}^0_{\text{fin.}}-\tilde{p}^z_{\text{fin.}}}\right) \neq Y$. This is accounted for by rescaling the colliding partons' energies and momentum fractions as follows

$$\tilde{p}_a = \left(\frac{1}{2}\sqrt{\tilde{s}}e^{\tilde{Y}}, 0, 0, \frac{1}{2}\sqrt{\tilde{s}}e^{\tilde{Y}}\right), \qquad \tilde{p}_b = \left(\frac{1}{2}\sqrt{\tilde{s}}e^{\tilde{Y}}, 0, 0, -\frac{1}{2}\sqrt{\tilde{s}}e^{\tilde{Y}}\right). \tag{4.17}$$

In the case of an initial-state clustering instead, one removes the final state parton that is closer to the beam (i.e. the one with smallest transverse momentum, dubbed emitted). The colour-neutral particles in the final state and all the other coloured partons but the one that has the smallest transverse momentum among the remaining ones, called next-to-softest (nts.), are instead left unchanged. It is in fact necessary to modify the transverse momentum of at least one of the remaining partons in order to absorb the transverse momentum of the removed emission, without modifying the colour-neutral system. The z-component of this parton is preserved and its energy is corrected to maintain it on-shell. In formulae

$$\tilde{p}_i = p_i \quad \text{for } i \neq \text{emi.}, \text{nts.} \qquad \text{and} \qquad \tilde{p}_{\text{nts.}} = \left(\tilde{p}^0_{\text{nts.}}, -\sum_{i\neq\text{nts.}} \tilde{p}^x_i, -\sum_{i\neq\text{nts.}} \tilde{p}^y_i, p^z_{\text{nts.}}\right),$$

where $\tilde{p}^0_{\text{nts.}} = \sqrt{(\tilde{p}^x_{\text{nts.}})^2 + (\tilde{p}^y_{\text{nts.}})^2 + (p^z_{\text{nts.}})^2}$. At this point one can again rescale the initial state momenta as in eq. (4.17) to accommodate for the change in the total energy and rapidity of $\tilde{p}_{\text{fin.}}$. We point out that both these mappings actually preserve the full four-momentum of the colour-singlet system, not only its transverse components. This means that any observable which is entirely determined by the momenta of the colour-singlet system or by its decay product (e.g. the leptons coming from the Z decay) will exactly be preserved by the projection and will therefore not receive any additional fiducial power correction.

In figure 6 we compare the $\mathcal{O}({\alpha_s}^3)$ corrections obtained by NNLOJET to those obtained by GENEVA with the nonlocal subtraction and including the FPCs for the q_T and $\mathcal{T}_0$ distributions. We observe the same good level of agreement both for an observable like q_T which is preserved by the P2B mapping as well as for $\mathcal{T}_0$, which is instead not preserved and subject to FPCs. In a similar fashion we compare the distributions of the decay products of the vector boson with a cut in q_T in figure 7 and with a cut in $\mathcal{T}_0$ in figure 8. Due to the complete preservation of the entire four momentum of the vector boson and of its decay products in the P2B mapping, the complete distributions in figure 7 are preserved. This is not the case for the distributions in figure 8, due to the cut on $\mathcal{T}_0$. We observe nonetheless a very good agreement with NNLOJET for both the cases.

We also notice a difference in the size of the statistical errors on the leptonic distributions compared to the one on the inclusive cross section in figure 4 for the same value of the cut in q_T or $\mathcal{T}_0$. Indeed, by calculating the NNLOJET cross section integrating over the bins of the leptonic distributions, one would find compatible results with a smaller error. This is likely a consequence of the NNLOJET treatment of outliers, as described in [58, 100], which is applied on a bin-to-bin basis. On the other hand, GENEVA does apply a trimming procedure to discard runs classified as outliers, but at the level of the fiducial cross section only. This preserves the statistical error of the integrated cross section, at the expense of larger errors in leptonic distributions.

JHEP01(2026)065

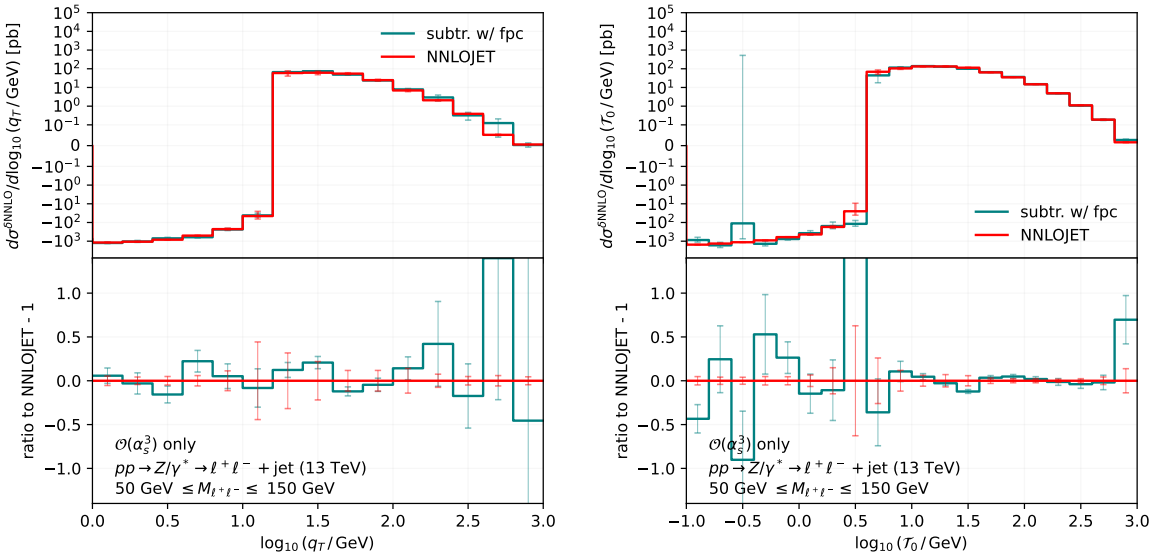

Figure 6. Comparison with NNLOJET of the Z+jet $\mathcal{O}(\alpha_s{}^3)$ corrections for the q_T (left) and $\mathcal{T}_0$ (right) differential distributions within the subtraction implementation including FPCs.

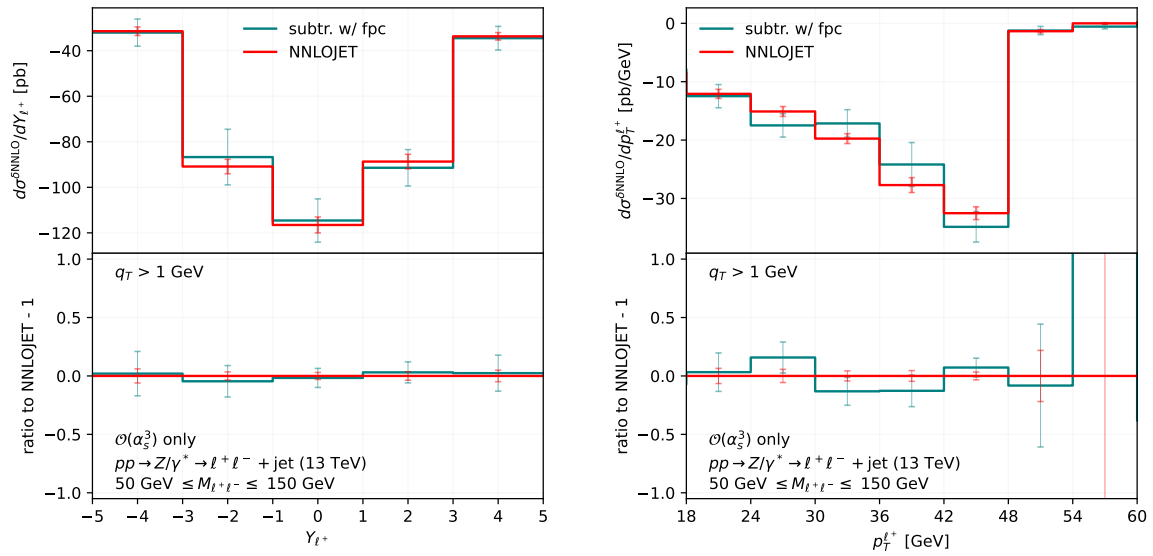

Figure 7. Comparison with NNLOJET of the Z+jet $\mathcal{O}(\alpha_s{}^3)$ corrections for the rapidity Y_{ℓ^+} (left) and transverse momentum $p_T^{\ell^+}$ (right) differential distributions of the positively charged lepton with a cut $q_T > 1\,\text{GeV}$, within the subtraction implementation including FPCs.

JHEP01(2026)065

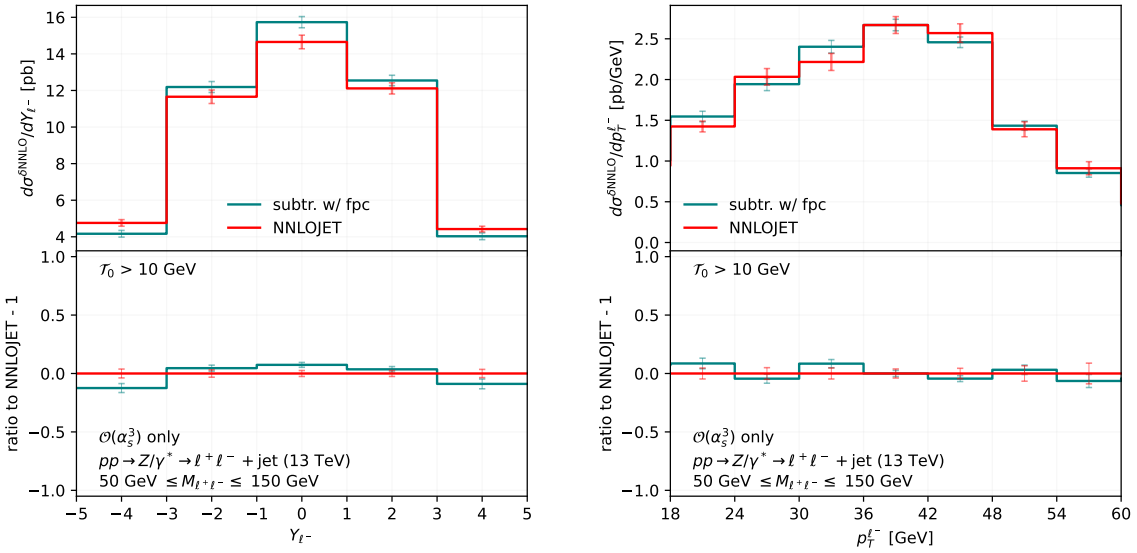

Figure 8. Comparison with NNLOJET of the Z+jet $\mathcal{O}(\alpha_s{}^3)$ corrections for the rapidity Y_{ℓ^-} (left) and transverse momentum $p_T^{\ell^-}$ (right) differential distributions of the negatively charged lepton with a cut $\mathcal{T}_0 > 10\,\text{GeV}$, within the subtraction implementation including FPCs.

5 Extension to higher orders

5.1 Validation of q_T and $\mathcal{T}_0$ spectra against $\mathcal{O}(\alpha_s{}^3)$ singular predictions

A crucial benefit of nonlocal subtractions is that the QCD IR singularities, present in the intermediate steps of a calculation, are mapped to a single variable and the counterterms are given in terms of the singular limits of physical cross sections. This renders such methods particularly appealing for higher-order predictions, because they are only limited by the availability of the perturbative ingredients that enter the 'subtraction' cross section. This is opposed to local subtractions, where disentangling the various (overlapping) singular regions and constructing appropriate (integrated) subtraction counter-terms has been proved to be a formidable task, although recent improvements suggest that their full automation at NNLO might not be far away [101–103].

On the other hand, it is a known fact that the residual dependence on the technical cut-off $\mathcal{T}_\delta$ in nonlocal subtractions affects the lower range of validity for the predictions of observables that are considered to be hard scales of the process. Two examples are the transverse momentum spectrum (q_T) of the colour-singlet system and the zero-jettiness ($\mathcal{T}_0$) resolution variables that, when they are evaluated at extremely small values, show a strong dependence on $\mathcal{T}_\delta$. Thus, as part of our NNLO validation for the Z+jet process, it is of outmost importance to quantitatively study the limitations of the GENEVA predictions when employing a certain cut-off value $\mathcal{T}_\delta$ in the $\mathcal{T}_1$ subtractions. In particular, in order to extend the value of $\mathcal{T}_\delta$ to lower values, while avoiding to violate the assumptions behind the factorization theorem for $\mathcal{T}_1$, which requires $\mathcal{T}_1$ to be much smaller than any other scale in the problem, including $\mathcal{T}_0$ or q_T, here we explore the possibility to change the definition

$$\mathcal{T}_\delta(\Phi_M) = \min\left\{\mathcal{T}_0(\Phi_M)/2, g(q_T(\Phi_M))\right\} \text{ with } g(x) \quad = 10^{-5}\cdot\left(1+10^{-3+6/(1+\exp(-2\sqrt[3]{x}))^5}\right),$$

JHEP01(2026)065

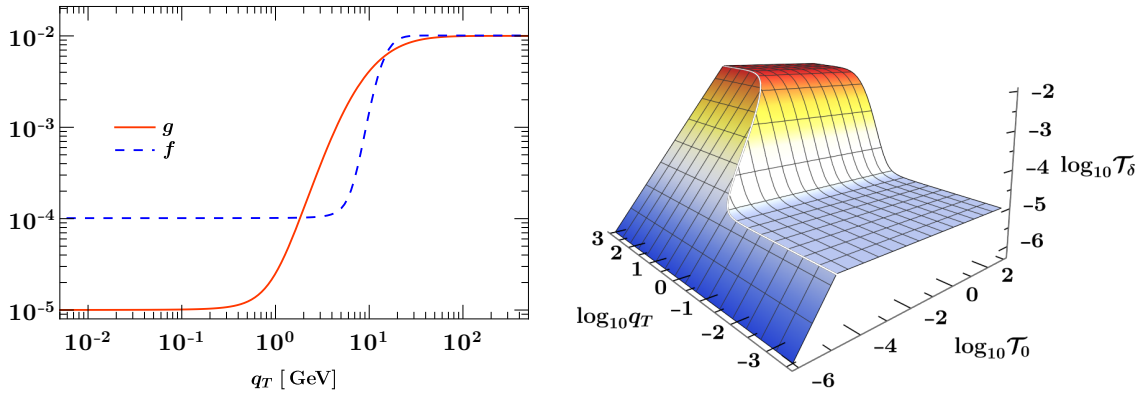

Figure 9. Comparison of the functional forms for the dynamical cut (left) and complete dependence of the new $\mathcal{T}_\delta$ on $\mathcal{T}_0$ and q_T (right).

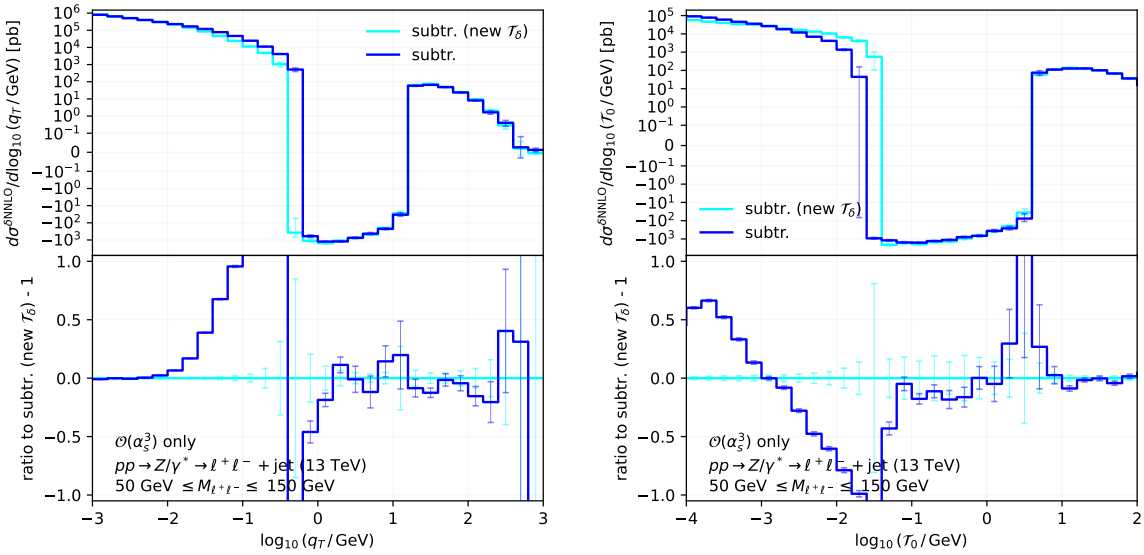

Figure 10. Comparison of the GENEVA results for the Z+jet $\mathcal{O}({\alpha_s}^3)$ corrections for the q_T (left) and $\mathcal{T}_0$ (right) differential distributions between different choices for the dynamical infrared cutoff within a subtraction implementation.

which interpolates the effective $\mathcal{T}_\delta$ between 10^{-5} and 10^{-2} when q_T varies between 0 and 100 GeV. In the left panel of figure 9 we show the comparison between the functional forms for the dynamical cut on $\mathcal{T}_\delta$ used in the previous section, compared to the new form, which can reach the smaller value of 10^{-5} GeV for values of $q_T \lesssim 1$ GeV. In the right panel of the same figure we show the new full $\mathcal{T}_\delta$ dependence on both $\mathcal{T}_0$ and q_T. As for the previous functional form, when $\mathcal{T}_0(\Phi_M) < 2g(q_T(\Phi_M))$ one has $\mathcal{T}_\delta = \mathcal{T}_1^{\text{cut}} = \mathcal{T}_0/2$ and the nonlocal subtraction falls back to be a pure slicing calculation. We compare the results for this new choice of the infrared cutoff with those used for the predictions in the previous sections in figure 10.

We first notice how the curves are identical for values of $q_T \gtrsim 1$ GeV and $\mathcal{T}_0 \gtrsim 0.1$ GeV, thus ensuring that the dynamical cutoff employed in the previous sections is correct for the

JHEP01(2026)065

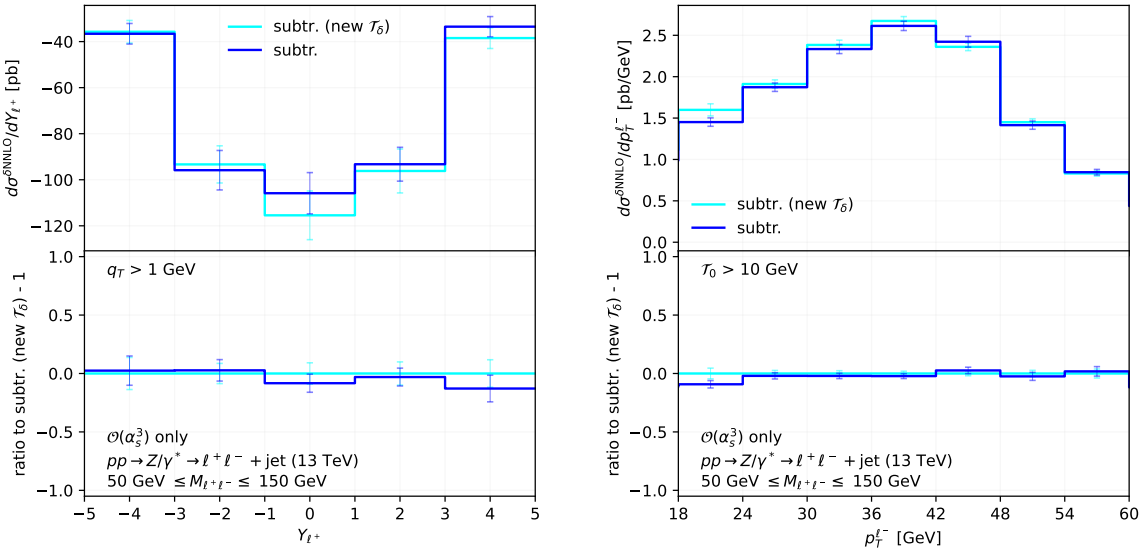

Figure 11. Comparison of the Z+jet $\mathcal{O}(\alpha_s{}^3)$ differential corrections for the rapidity Y_{ℓ^+} (left) of the positively charged lepton with a cut $q_T > 1\,\text{GeV}$ and of the transverse momentum $p_T^{\ell^-}$ (right) of the negatively charged lepton with a cut $\mathcal{T}_0 > 10\,\text{GeV}$, within the subtraction implementation for different values of the infrared cutoff $\mathcal{T}_\delta$.

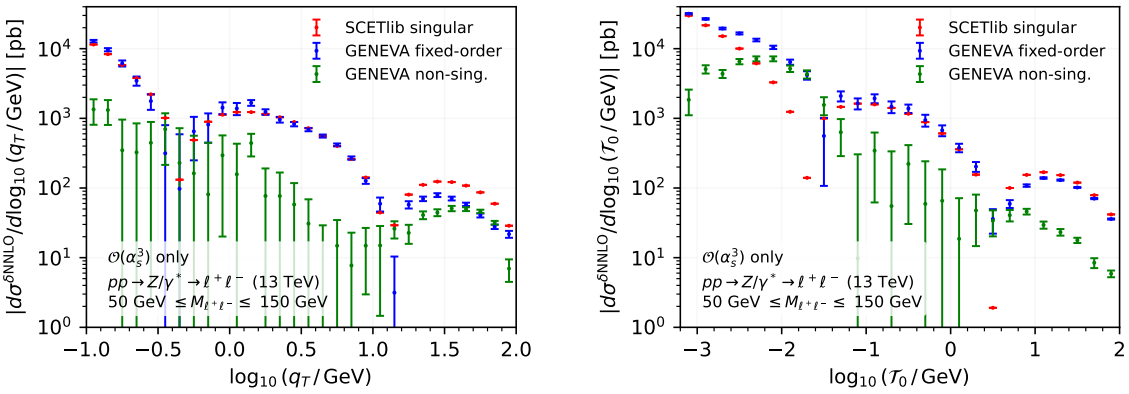

Figure 12. Validation of GENEVA $\mathcal{O}(\alpha_s{}^3)$ Z+jet predictions in small-q_T (left) and small-$\mathcal{T}_0$ (right) regions against singular predictions from SCETLIB with the nonsingular contribution (green) corresponding to their difference.

observables studied there. This is further confirmed by the comparison of the differential distribution of the Z decay products in figure 11.

For smaller values of q_T or $\mathcal{T}_0$, however, we notice a considerable shift between the predictions obtained with the different dynamical cuts. This behaviour is expected, because for those small values of q_T or $\mathcal{T}_0$ the previous form of the infrared cutoff $\mathcal{T}_\delta$ enters a kinematic regime where the factorization theorem for $\mathcal{T}_1$ is no longer valid.

In this situation one might ask how to determine the correct form for the dynamical cut and how low one can push the infrared cutoff, considering that when the cutoff is pushed

JHEP01(2026)065

to extremely low values the NLO calculation above the cut becomes very unstable, being evaluated close to its IR limits. The correct way to address this question is to use as IR cutoff the largest value that keeps the NLO calculation above the cut stable while capturing the correct singular behaviour of the q_T or $\mathcal{T}_0$ spectra. In order to further explain this point, in figure 12 we show the $\mathcal{O}({\alpha_s}^3)$ coefficient for the q_T (left) and the $\mathcal{T}_0$ (right) spectrum from GENEVA (blue) and from SCETLIB (red) [23, 24, 46, 104, 105], where the latter predicts the singular cross section of the corresponding resolution variable. The singular cross section is known to dominate in the limits $q_T, \mathcal{T}_0 \to 0$ due to large, unresummed Sudakov double-logarithms and its difference to the fixed-order cross section, here denoted as 'nonsingular' (green), is expected to show a power suppressed behaviour [89, 91, 106–114].

It is evident for both resolution variables that the nonsingular cross section is significantly suppressed for low values of q_T and $\mathcal{T}_0$, although a clear power law is hard to discern. This is partially attributed to the fact that the coefficients have two zero-crossings deep in the singular region ($q_T \simeq 0.4\,\text{GeV}, 10\,\text{GeV}$ and $\mathcal{T}_0 \simeq 2 \times 10^{-2}\,\text{GeV}, 3\,\text{GeV}$), and it is thus numerically challenging to obtain the expected quadratic (linear) power suppression for q_T ($\mathcal{T}_0$) in the region in-between. In contrast, a downward trend for $\mathcal{T}_0 \lesssim 10^{-2}\,\text{GeV}$ can be seen but the effect of the technical cut-offs of the NLO_1 calculation become significant below $\mathcal{T}_0 \lesssim 7 \times 10^{-4}\,\text{GeV}$, which effectively defines the lowest valid value of the $\mathcal{T}_0$ fixed-order results of GENEVA for this choice of $\mathcal{T}_\delta$ and the NLO technical cuts. Similar conclusions are also drawn for q_T, with the lowest valid value at $q_T \simeq 0.2\,\text{GeV}$.

We stress though, that employing even lower values of the technical cut-off $\mathcal{T}_\delta$ would allow us in principle to push the range of validity for the q_T and $\mathcal{T}_0$ spectra at even smaller values, but this has to be balanced with the instability of the NLO calculation with reduced technical cuts. We remind the reader that even for local subtraction methods is computationally challenging to properly describe the small q_T or $\mathcal{T}_0$ regions.

Finally, in addition to the zero-crossings of the coefficients, we remind the known fact that for this process, the aggregate of all partonic channels is known to exhibit significant numerical cancellations which potentially further obscure the expected power-suppressed trend of the nonsingular. A more careful treatment could involve the inspection of the nonsingular cross section for each partonic channel separately, as done e.g. in refs. [48, 95, 115]. This will potentially allow us to unravel the channel-specific scaling trend of the nonsingular cross section. We leave this study to future work.

5.2 Extension to N^{3}LO colour-singlet hadroproduction

Having validated the nonsingular spectrum against the N^{3}LL singular predictions and given the availability of all the three-loop boundary terms necessary for the N^{3}LL$'$ resummation for both q_T and $\mathcal{T}_0$ for colour-singlet hadroproduction [116–118], we can extend eq. (2.12) to one order higher, in order to calculate the N^{3}LO fully-exclusive corrections. Using $\mathcal{T}_0$ as

JHEP01(2026)065

example resolution variable (but the formula applies equally to q_T) we obtain

$$\begin{aligned}\mathcal{O}_{\delta\mathrm{N^3LO}}(\Phi_0) = &\frac{\mathrm{d}\Sigma^{\delta\mathrm{N^3LO}}_{0,\mathrm{sub.}}}{\mathrm{d}\Phi_0}(\mathcal{T}_0^{\mathrm{cut}})\,\mathcal{O}(\Phi_0) \\ &+\int\frac{\mathrm{d}\Phi_1}{\mathrm{d}\Phi_0}\Big[\frac{\mathrm{d}\sigma_1^{\delta\mathrm{NNLO}}}{\mathrm{d}\Phi_1}-\frac{\mathrm{d}\sigma^{\delta\mathrm{N^3LO}}_{0,\mathrm{sub.}}}{\mathrm{d}\Phi_0\,\mathrm{d}\mathcal{T}_0}\,P(\Phi_1)\,\theta(\mathcal{T}_0(\Phi_1)<\mathcal{T}_0^{\mathrm{cut}})\Big] \\ &\quad\times\mathcal{O}(\Phi_0)\;\theta\Big(\mathcal{T}_0(\Phi_{X=\{1,2,3\}})>\mathcal{T}_{0,\delta}\Big) \\ &+\int\frac{\mathrm{d}\Phi_1}{\mathrm{d}\Phi_0}\frac{\mathrm{d}\sigma_1^{\delta\mathrm{NNLO}}}{\mathrm{d}\Phi_1}\Big[\mathcal{O}(\Phi_{X=\{1,2,3\}})-\mathcal{O}(\Phi_0)\Big]\,. \\ &+\text{inclusive power corrections in }\mathcal{T}_{0,\delta}\,,\end{aligned} \tag{5.1}$$

where the inclusive NNLO cross-section at fixed underlying-Born kinematics in the second and last line above, $\mathrm{d}\sigma_1^{\delta\mathrm{NNLO}}/\mathrm{d}\Phi_1\;\mathcal{O}(\Phi_0)$, can be obtained by projecting $\Phi_{X=\{1,2,3\}}\to\Phi_0$ and evaluating the observable on the Φ_0 configuration in eq. (2.12), giving

$$\begin{aligned}\frac{\mathrm{d}\sigma_1^{\delta\mathrm{NNLO}}}{\mathrm{d}\Phi_1}\;\mathcal{O}(\Phi_0) = \mathcal{O}(\Phi_0)\;\Bigg\{&\frac{\mathrm{d}\Sigma^{\delta\mathrm{NNLO}}_{1,\mathrm{sub.}}}{\mathrm{d}\Phi_1}(\mathcal{T}_1^{\mathrm{cut}}) \\ &+\int\frac{\mathrm{d}\Phi_2}{\mathrm{d}\Phi_1}\Big[\frac{\mathrm{d}\sigma_2^{\delta\mathrm{NLO}}}{\mathrm{d}\Phi_2}-\frac{\mathrm{d}\sigma^{\delta\mathrm{NNLO}}_{1,\mathrm{sub.}}}{\mathrm{d}\Phi_1\,\mathrm{d}\mathcal{T}_1}\,P(\Phi_2)\,\theta(\mathcal{T}_1(\Phi_2)<\mathcal{T}_1^{\mathrm{cut}})\Big] \\ &\quad\times\;\theta\Big(\mathcal{T}_1(\Phi_{X=\{2,3\}})>\mathcal{T}_{1,\delta}\Big) \\ &+\text{inclusive power corrections in }\mathcal{T}_{1,\delta}\Bigg\}\,.\end{aligned} \tag{5.2}$$

The dependence on the observable must instead be retained during the evaluation of the $\mathrm{d}\sigma_1^{\delta\mathrm{NNLO}}/\mathrm{d}\Phi_1\;\mathcal{O}(\Phi_{X=\{1,2,3\}})$ contributions appearing in the last line of eq. (5.1), in order to properly account for the fiducial power corrections. The implementation details, the numerical dependence on the neglected power corrections in both $\mathcal{T}_{0,\delta}$ and $\mathcal{T}_{1,\delta}$ and the results will be discussed in a future publication.

6 Conclusions

In this work, we present a novel calculation of fully-exclusive NNLO QCD corrections, which employs genuine nonlocal subtractions based on N-jettiness resolution variables, in combination with the Projection-to-Born (P2B) method, to effectively handle fiducial power corrections (FPCs) in a fully-differential context. We show numerical results for both colour-singlet and colour-singlet+jet processes within the GENEVA framework. To the best of our knowledge, this represents the first implementation of such a nonlocal subtraction method within a general-purpose event generator and the first application of the P2B method for processes with final-state jets which are divergent at the Born level.

We have carefully addressed the challenges associated with the usage of a dynamic resolution cutoff, which is necessary to correctly handle the complications associated with multi-scale problems, providing prescriptions for implementing subtraction terms that preserve phase-space constraints and accommodate dynamic cuts. We demonstrated the robustness

JHEP01(2026)065

and accuracy of our implementation through detailed studies of neutral Drell-Yan and Z+jet production at the LHC, validating our results against those obtained from NNLOJET. The inclusion of FPCs further improves the agreement in fiducial regions, underscoring the importance of these effects in precision collider phenomenology. Our results show that the present subtraction-based implementation yields marginally better numerical convergence and lower integration errors than traditional slicing approaches, even under demanding kinematic constraints. Furthermore, the ability to incorporate the leading next-to-leading-power logarithms in the subtractions allows for more stable predictions with less sensitivity to the infrared resolution parameter.

Looking ahead, our approach lays the groundwork for future extensions. In particular, the framework presented here is well-suited for the computation of fully-differential N^{3}LO corrections for colour-singlet production at hadron colliders, which are of paramount importance for matching the precision of the upcoming HL-LHC data. Moreover, the formalism can be naturally extended to processes with higher jet multiplicities or to include electroweak corrections. We anticipate that this work will be a key step toward the consistent inclusion of NNLO (and beyond) corrections within NNLO+PS event generators for processes with final-state jets, allowing for more precise theoretical predictions and an improved understanding of QCD dynamics at high-energy colliders.

Acknowledgments

We are grateful to F. Tackmann, J.K.L. Michel, G. Vita and A. Huss for discussions. We also thank our GENEVA collaborators A. Gavardi, M.A. Lim, D. Napoletano and G. Marinelli for valuable exchanges and their work on the GENEVA code. We acknowledge financial support, supercomputing resources and support from ICSC — Centro Nazionale di Ricerca in High Performance Computing, Big Data and Quantum Computing — and hosting entity, funded by European Union — NextGenerationEU.

Data Availability Statement. This article has no associated data or the data will not be deposited.

Code Availability Statement. This article has no associated code or the code will not be deposited.

Open Access. This article is distributed under the terms of the Creative Commons Attribution License (CC-BY4.0), which permits any use, distribution and reproduction in any medium, provided the original author(s) and source are credited.

References

[1] CMS collaboration, *Measurement of the inclusive cross sections for W and Z boson production in proton-proton collisions at* $\sqrt{s} = 5.02$ *and 13 TeV*, *JHEP* **04** (2025) 162 [arXiv:2408.03744] [INSPIRE].

[2] ATLAS collaboration, *Measurement of* $W^{\pm}$*-boson differential cross-sections in proton-proton collisions with low pile-up data at* $\sqrt{s} = 5.02$ *TeV and* 13 *TeV with the ATLAS detector*, *Eur. Phys. J. C* **85** (2025) 729 [arXiv:2502.09403] [INSPIRE].

JHEP01(2026)065

[3] ATLAS collaboration, *Precise measurements of W- and Z-boson transverse momentum spectra with the ATLAS detector using pp collisions at* $\sqrt{s} = 5.02$ *TeV and 13 TeV*, *Eur. Phys. J. C* **84** (2024) 1126 [arXiv:2404.06204] [INSPIRE].

[4] ATLAS collaboration, *Measurement of double-differential charged-current Drell-Yan cross-sections at high transverse masses in pp collisions at* $\sqrt{s} = 13$ *TeV with the ATLAS detector*, *JHEP* **07** (2025) 026 [arXiv:2502.21088] [INSPIRE].

[5] CMS collaboration, *Measurements of the inclusive W and Z boson production cross sections and their ratios in proton-proton collisions at* $\sqrt{s} = 13.6$ *TeV*, arXiv:2503.09742 [INSPIRE].

[6] S. Camarda, G. Ferrera and M. Schott, *Determination of the strong-coupling constant from the Z-boson transverse-momentum distribution*, *Eur. Phys. J. C* **84** (2024) 39 [arXiv:2203.05394] [INSPIRE].

[7] ATLAS collaboration, *A precise determination of the strong-coupling constant from the recoil of Z bosons with the ATLAS experiment at* $\sqrt{s} = 8$ *TeV*, arXiv:2309.12986 [INSPIRE].

[8] CMS collaboration, *Search for new particles in events with energetic jets and large missing transverse momentum in proton-proton collisions at* $\sqrt{s} = 13$ *TeV*, *JHEP* **11** (2021) 153 [arXiv:2107.13021] [INSPIRE].

[9] ATLAS collaboration, *Search for new phenomena in events with an energetic jet and missing transverse momentum in pp collisions at* $\sqrt{s} = 13$ *TeV with the ATLAS detector*, *Phys. Rev. D* **103** (2021) 112006 [arXiv:2102.10874] [INSPIRE].

[10] ATLAS collaboration, *Measurement of the W-boson mass in pp collisions at* $\sqrt{s} = 7$ *TeV with the ATLAS detector*, *Eur. Phys. J. C* **78** (2018) 110 [*Erratum ibid.* **78** (2018) 898] [arXiv:1701.07240] [INSPIRE].

[11] LHCb collaboration, *Measurement of the W boson mass*, *JHEP* **01** (2022) 036 [arXiv:2109.01113] [INSPIRE].

[12] CDF collaboration, *High-precision measurement of the W boson mass with the CDF II detector*, *Science* **376** (2022) 170 [INSPIRE].

[13] CMS collaboration, *High-precision measurement of the W boson mass with the CMS experiment at the LHC*, arXiv:2412.13872 [INSPIRE].

[14] ATLAS collaboration, *Measurement of the W-boson mass and width with the ATLAS detector using proton–proton collisions at* $\sqrt{s} = 7$ *TeV*, *Eur. Phys. J. C* **84** (2024) 1309 [arXiv:2403.15085] [INSPIRE].

[15] F. Caola et al., *The Path forward to* N^3LO, in the proceedings of the *Snowmass 2021*, Seattle, U.S.A., July 17–26 (2022) [arXiv:2203.06730] [INSPIRE].

[16] X. Chen et al., *Transverse mass distribution and charge asymmetry in W boson production to third order in QCD*, *Phys. Lett. B* **840** (2023) 137876 [arXiv:2205.11426] [INSPIRE].

[17] J. Campbell and T. Neumann, *Third order QCD predictions for fiducial W-boson production*, *JHEP* **11** (2023) 127 [arXiv:2308.15382] [INSPIRE].

[18] X. Chen et al., *Dilepton Rapidity Distribution in Drell-Yan Production to Third Order in QCD*, *Phys. Rev. Lett.* **128** (2022) 052001 [arXiv:2107.09085] [INSPIRE].

[19] X. Chen et al., *Third-Order Fiducial Predictions for Drell-Yan Production at the LHC*, *Phys. Rev. Lett.* **128** (2022) 252001 [arXiv:2203.01565] [INSPIRE].

JHEP01(2026)065

[20] T. Neumann and J. Campbell, *Fiducial Drell-Yan production at the LHC improved by transverse-momentum resummation at N4LLp+N3LO*, *Phys. Rev. D* **107** (2023) L011506 [arXiv:2207.07056] [INSPIRE].

[21] L. Cieri et al., *Higgs boson production at the LHC using the q_T subtraction formalism at N^3LO QCD*, *JHEP* **02** (2019) 096 [arXiv:1807.11501] [INSPIRE].

[22] X. Chen et al., *Fully Differential Higgs Boson Production to Third Order in QCD*, *Phys. Rev. Lett.* **127** (2021) 072002 [arXiv:2102.07607] [INSPIRE].

[23] G. Billis et al., *Higgs pT Spectrum and Total Cross Section with Fiducial Cuts at Third Resummed and Fixed Order in QCD*, *Phys. Rev. Lett.* **127** (2021) 072001 [arXiv:2102.08039] [INSPIRE].

[24] G. Billis, J.K.L. Michel and F.J. Tackmann, *Drell-Yan transverse-momentum spectra at N^3LL' and approximate N^4LL with SCETlib*, *JHEP* **02** (2025) 170 [arXiv:2411.16004] [INSPIRE].

[25] R. Boughezal et al., *Higgs boson production in association with a jet at next-to-next-to-leading order in perturbative QCD*, *JHEP* **06** (2013) 072 [arXiv:1302.6216] [INSPIRE].

[26] A. Gehrmann-De Ridder, T. Gehrmann and E.W.N. Glover, *Antenna subtraction at NNLO*, *JHEP* **09** (2005) 056 [hep-ph/0505111] [INSPIRE].

[27] M. Czakon, *A novel subtraction scheme for double-real radiation at NNLO*, *Phys. Lett. B* **693** (2010) 259 [arXiv:1005.0274] [INSPIRE].

[28] M. Czakon, *Double-real radiation in hadronic top quark pair production as a proof of a certain concept*, *Nucl. Phys. B* **849** (2011) 250 [arXiv:1101.0642] [INSPIRE].

[29] R. Boughezal et al., *Z-boson production in association with a jet at next-to-next-to-leading order in perturbative QCD*, *Phys. Rev. Lett.* **116** (2016) 152001 [arXiv:1512.01291] [INSPIRE].

[30] S. Catani and M. Grazzini, *An NNLO subtraction formalism in hadron collisions and its application to Higgs boson production at the LHC*, *Phys. Rev. Lett.* **98** (2007) 222002 [hep-ph/0703012] [INSPIRE].

[31] M. Grazzini, S. Kallweit and M. Wiesemann, *Fully differential NNLO computations with MATRIX*, *Eur. Phys. J. C* **78** (2018) 537 [arXiv:1711.06631] [INSPIRE].

[32] J.M. Campbell, R.K. Ellis and S. Seth, *Non-local slicing approaches for NNLO QCD in MCFM*, *JHEP* **06** (2022) 002 [arXiv:2202.07738] [INSPIRE].

[33] S. Abreu et al., *Quark and gluon two-loop beam functions for leading-jet p_T and slicing at NNLO*, *JHEP* **04** (2023) 127 [arXiv:2207.07037] [INSPIRE].

[34] J. Gaunt, M. Stahlhofen, F.J. Tackmann and J.R. Walsh, *N-jettiness Subtractions for NNLO QCD Calculations*, *JHEP* **09** (2015) 058 [arXiv:1505.04794] [INSPIRE].

[35] R. Boughezal, C. Focke, X. Liu and F. Petriello, *W-boson production in association with a jet at next-to-next-to-leading order in perturbative QCD*, *Phys. Rev. Lett.* **115** (2015) 062002 [arXiv:1504.02131] [INSPIRE].

[36] R. Boughezal et al., *Color singlet production at NNLO in MCFM*, *Eur. Phys. J. C* **77** (2017) 7 [arXiv:1605.08011] [INSPIRE].

[37] J. Campbell and T. Neumann, *Precision Phenomenology with MCFM*, *JHEP* **12** (2019) 034 [arXiv:1909.09117] [INSPIRE].

[38] J. Gao, C.S. Li and H.X. Zhu, *Top Quark Decay at Next-to-Next-to Leading Order in QCD*, *Phys. Rev. Lett.* **110** (2013) 042001 [arXiv:1210.2808] [INSPIRE].

JHEP01(2026)065

[39] Z.L. Liu and J. Gao, *s -channel single top quark production and decay at next-to-next-to-leading-order in QCD*, *Phys. Rev. D* **98** (2018) 071501 [arXiv:1807.03835] [INSPIRE].

[40] L. Buonocore, S. Kallweit, L. Rottoli and M. Wiesemann, *Linear power corrections for two-body kinematics in the qT subtraction formalism*, *Phys. Lett. B* **829** (2022) 137118 [arXiv:2111.13661] [INSPIRE].

[41] S. Camarda, L. Cieri and G. Ferrera, *Fiducial perturbative power corrections within the $\mathbf{q}_T$ subtraction formalism*, *Eur. Phys. J. C* **82** (2022) 575 [arXiv:2111.14509] [INSPIRE].

[42] M. Cacciari et al., *Fully Differential Vector-Boson-Fusion Higgs Production at Next-to-Next-to-Leading Order*, *Phys. Rev. Lett.* **115** (2015) 082002 [*Erratum ibid.* **120** (2018) 139901] [arXiv:1506.02660] [INSPIRE].

[43] M.A. Ebert and F.J. Tackmann, *Impact of isolation and fiducial cuts on q_T and N-jettiness subtractions*, *JHEP* **03** (2020) 158 [arXiv:1911.08486] [INSPIRE].

[44] J. Campbell, T. Neumann and G. Vita, *Projection-to-Born-improved subtractions at NNLO*, *JHEP* **05** (2025) 172 [arXiv:2408.05265] [INSPIRE].

[45] S. Alioli et al., *Refining the GENEVA method for Higgs boson production via gluon fusion*, *JHEP* **05** (2023) 128 [arXiv:2301.11875] [INSPIRE].

[46] G. Billis, M.A. Ebert, J.K.L. Michel and F.J. Tackmann, *A toolbox for q_T and 0-jettiness subtractions at N^3LO*, *Eur. Phys. J. Plus* **136** (2021) 214 [arXiv:1909.00811] [INSPIRE].

[47] S. Alioli et al., *N3LL resummation of one-jettiness for Z-boson plus jet production at hadron colliders*, *Phys. Rev. D* **109** (2024) 094009 [arXiv:2312.06496] [INSPIRE].

[48] I. Moult et al., *Subleading Power Corrections for N-Jettiness Subtractions*, *Phys. Rev. D* **95** (2017) 074023 [arXiv:1612.00450] [INSPIRE].

[49] R. Boughezal et al., *Higgs boson production in association with a jet at NNLO using jettiness subtraction*, *Phys. Lett. B* **748** (2015) 5 [arXiv:1505.03893] [INSPIRE].

[50] J.M. Campbell, R.K. Ellis and S. Seth, *H + 1 jet production revisited*, *JHEP* **10** (2019) 136 [arXiv:1906.01020] [INSPIRE].

[51] S. Alioli et al., *Drell-Yan production at NNLL'+NNLO matched to parton showers*, *Phys. Rev. D* **92** (2015) 094020 [arXiv:1508.01475] [INSPIRE].

[52] S. Alioli et al., *Higgsstrahlung at NNLL'+NNLO matched to parton showers in GENEVA*, *Phys. Rev. D* **100** (2019) 096016 [arXiv:1909.02026] [INSPIRE].

[53] S. Alioli et al., *Resummed predictions for hadronic Higgs boson decays*, *JHEP* **04** (2021) 254 [arXiv:2009.13533] [INSPIRE].

[54] S. Alioli et al., *Precise predictions for photon pair production matched to parton showers in GENEVA*, *JHEP* **04** (2021) 041 [arXiv:2010.10498] [INSPIRE].

[55] S. Alioli et al., *Next-to-next-to-leading order event generation for Z boson pair production matched to parton shower*, *Phys. Lett. B* **818** (2021) 136380 [arXiv:2103.01214] [INSPIRE].

[56] T. Cridge, M.A. Lim and R. Nagar, *$W\gamma$ production at NNLO+PS accuracy in Geneva*, *Phys. Lett. B* **826** (2022) 136918 [arXiv:2105.13214] [INSPIRE].

[57] S. Alioli et al., *Double Higgs production at NNLO interfaced to parton showers in GENEVA*, *JHEP* **06** (2023) 205 [arXiv:2212.10489] [INSPIRE].

JHEP01(2026)065

[58] NNLOJET collaboration, *NNLOJET: a parton-level event generator for jet cross sections at NNLO QCD accuracy*, arXiv:2503.22804 [INSPIRE].

[59] F.A. Berends, W.T. Giele and H. Kuijf, *Exact Expressions for Processes Involving a Vector Boson and Up to Five Partons*, *Nucl. Phys. B* **321** (1989) 39 [INSPIRE].

[60] Z. Bern, L.J. Dixon and D.A. Kosower, *One loop amplitudes for e^+e^- to four partons*, *Nucl. Phys. B* **513** (1998) 3 [hep-ph/9708239] [INSPIRE].

[61] R. Boughezal, A. Gehrmann-De Ridder and M. Ritzmann, *Antenna subtraction at NNLO with hadronic initial states: double real radiation for initial-initial configurations with two quark flavours*, *JHEP* **02** (2011) 098 [arXiv:1011.6631] [INSPIRE].

[62] A. Buckley et al., *LHAPDF6: parton density access in the LHC precision era*, *Eur. Phys. J. C* **75** (2015) 132 [arXiv:1412.7420] [INSPIRE].

[63] J. Currie, E.W.N. Glover and S. Wells, *Infrared Structure at NNLO Using Antenna Subtraction*, *JHEP* **04** (2013) 066 [arXiv:1301.4693] [INSPIRE].

[64] A. Daleo, T. Gehrmann and D. Maitre, *Antenna subtraction with hadronic initial states*, *JHEP* **04** (2007) 016 [hep-ph/0612257] [INSPIRE].

[65] A. Daleo, A. Gehrmann-De Ridder, T. Gehrmann and G. Luisoni, *Antenna subtraction at NNLO with hadronic initial states: initial-final configurations*, *JHEP* **01** (2010) 118 [arXiv:0912.0374] [INSPIRE].

[66] L.W. Garland et al., *The two loop QCD matrix element for $e^+e^- \to 3$ jets*, *Nucl. Phys. B* **627** (2002) 107 [hep-ph/0112081] [INSPIRE].

[67] L.W. Garland et al., *Two loop QCD helicity amplitudes for $e^+e^- \to$ three jets*, *Nucl. Phys. B* **642** (2002) 227 [hep-ph/0206067] [INSPIRE].

[68] R. Gauld et al., *Precise predictions for the angular coefficients in Z-boson production at the LHC*, *JHEP* **11** (2017) 003 [arXiv:1708.00008] [INSPIRE].

[69] R. Gauld et al., *Transverse momentum distributions in low-mass Drell-Yan lepton pair production at NNLO QCD*, *Phys. Lett. B* **829** (2022) 137111 [arXiv:2110.15839] [INSPIRE].

[70] T. Gehrmann and E. Remiddi, *Analytic continuation of massless two loop four point functions*, *Nucl. Phys. B* **640** (2002) 379 [hep-ph/0207020] [INSPIRE].

[71] T. Gehrmann and L. Tancredi, *Two-loop QCD helicity amplitudes for $q\bar{q} \to W^{\pm}\gamma$ and $q\bar{q} \to Z^0\gamma$*, *JHEP* **02** (2012) 004 [arXiv:1112.1531] [INSPIRE].

[72] T. Gehrmann and P.F. Monni, *Antenna subtraction at NNLO with hadronic initial states: real-virtual initial-initial configurations*, *JHEP* **12** (2011) 049 [arXiv:1107.4037] [INSPIRE].

[73] A. Gehrmann-De Ridder, T. Gehrmann and E.W.N. Glover, *Infrared structure of $e^+e^- \to 2$ jets at NNLO*, *Nucl. Phys. B* **691** (2004) 195 [hep-ph/0403057] [INSPIRE].

[74] A. Gehrmann-De Ridder, T. Gehrmann and E.W.N. Glover, *Gluon-gluon antenna functions from Higgs boson decay*, *Phys. Lett. B* **612** (2005) 49 [hep-ph/0502110] [INSPIRE].

[75] A. Gehrmann-De Ridder, T. Gehrmann and E.W.N. Glover, *Quark-gluon antenna functions from neutralino decay*, *Phys. Lett. B* **612** (2005) 36 [hep-ph/0501291] [INSPIRE].

[76] A. Gehrmann-De Ridder, T. Gehrmann, E.W.N. Glover and G. Heinrich, *Infrared structure of $e^+e^- \to 3$ jets at NNLO*, *JHEP* **11** (2007) 058 [arXiv:0710.0346] [INSPIRE].

JHEP01(2026)065

[77] A. Gehrmann-De Ridder, T. Gehrmann and M. Ritzmann, *Antenna subtraction at NNLO with hadronic initial states: double real initial-initial configurations*, *JHEP* **10** (2012) 047 [arXiv:1207.5779] [INSPIRE].

[78] A. Gehrmann-De Ridder et al., *Precise QCD predictions for the production of a Z boson in association with a hadronic jet*, *Phys. Rev. Lett.* **117** (2016) 022001 [arXiv:1507.02850] [INSPIRE].

[79] A. Gehrmann-De Ridder et al., *The NNLO QCD corrections to Z boson production at large transverse momentum*, *JHEP* **07** (2016) 133 [arXiv:1605.04295] [INSPIRE].

[80] A. Gehrmann-De Ridder et al., *NNLO QCD corrections for Drell-Yan p_T^Z and ϕ^* observables at the LHC*, *JHEP* **11** (2016) 094 [*Erratum ibid.* **10** (2018) 126] [arXiv:1610.01843] [INSPIRE].

[81] A. Gehrmann-De Ridder et al., *Vector Boson Production in Association with a Jet at Forward Rapidities*, *Eur. Phys. J. C* **79** (2019) 526 [arXiv:1901.11041] [INSPIRE].

[82] A. Gehrmann-De Ridder et al., *Precision phenomenology with fiducial cross sections in the triple-differential Drell-Yan process*, *JHEP* **05** (2023) 002 [arXiv:2301.11827] [INSPIRE].

[83] K. Hagiwara and D. Zeppenfeld, *Amplitudes for Multiparton Processes Involving a Current at e^+e^-, $e^\pm$ p, and Hadron Colliders*, *Nucl. Phys. B* **313** (1989) 560 [INSPIRE].

[84] S. Frixione, Z. Kunszt and A. Signer, *Three jet cross-sections to next-to-leading order*, *Nucl. Phys. B* **467** (1996) 399 [hep-ph/9512328] [INSPIRE].

[85] R. Frederix, S. Frixione, F. Maltoni and T. Stelzer, *Automation of next-to-leading order computations in QCD: The FKS subtraction*, *JHEP* **10** (2009) 003 [arXiv:0908.4272] [INSPIRE].

[86] NNPDF collaboration, *Parton distributions from high-precision collider data*, *Eur. Phys. J. C* **77** (2017) 663 [arXiv:1706.00428] [INSPIRE].

[87] F. Buccioni et al., *OpenLoops 2*, *Eur. Phys. J. C* **79** (2019) 866 [arXiv:1907.13071] [INSPIRE].

[88] ATLAS collaboration, *Measurement of the transverse momentum distribution of Drell-Yan lepton pairs in proton–proton collisions at $\sqrt{s} = 13$ TeV with the ATLAS detector*, *Eur. Phys. J. C* **80** (2020) 616 [arXiv:1912.02844] [INSPIRE].

[89] I.W. Stewart, F.J. Tackmann and W.J. Waalewijn, *Factorization at the LHC: From PDFs to Initial State Jets*, *Phys. Rev. D* **81** (2010) 094035 [arXiv:0910.0467] [INSPIRE].

[90] I.W. Stewart, F.J. Tackmann and W.J. Waalewijn, *The Quark Beam Function at NNLL*, *JHEP* **09** (2010) 005 [arXiv:1002.2213] [INSPIRE].

[91] I.W. Stewart, F.J. Tackmann and W.J. Waalewijn, *N-Jettiness: An Inclusive Event Shape to Veto Jets*, *Phys. Rev. Lett.* **105** (2010) 092002 [arXiv:1004.2489] [INSPIRE].

[92] R. Boughezal, X. Liu and F. Petriello, *Power Corrections in the N-jettiness Subtraction Scheme*, *JHEP* **03** (2017) 160 [arXiv:1612.02911] [INSPIRE].

[93] M.A. Ebert et al., *Power Corrections for N-Jettiness Subtractions at $\mathcal{O}(\alpha_s)$*, *JHEP* **12** (2018) 084 [arXiv:1807.10764] [INSPIRE].

[94] R. Boughezal, A. Isgrò and F. Petriello, *Next-to-leading-logarithmic power corrections for N-jettiness subtraction in color-singlet production*, *Phys. Rev. D* **97** (2018) 076006 [arXiv:1802.00456] [INSPIRE].

[95] I. Moult et al., *N -jettiness subtractions for $gg \to H$ at subleading power*, *Phys. Rev. D* **97** (2018) 014013 [arXiv:1710.03227] [INSPIRE].

JHEP01(2026)065

[96] G. Vita, *N^3LO power corrections for 0-jettiness subtractions with fiducial cuts*, *JHEP* **07** (2024) 241 [arXiv:2401.03017] [INSPIRE].

[97] J.M. Campbell, T. Neumann and C. Williams, *$Z\gamma$ Production at NNLO Including Anomalous Couplings*, *JHEP* **11** (2017) 150 [arXiv:1708.02925] [INSPIRE].

[98] S. Catani and B.R. Webber, *Infrared safe but infinite: Soft gluon divergences inside the physical region*, *JHEP* **10** (1997) 005 [hep-ph/9710333] [INSPIRE].

[99] M.A. Ebert, J.K.L. Michel, I.W. Stewart and F.J. Tackmann, *Drell-Yan q_T resummation of fiducial power corrections at N^3LL*, *JHEP* **04** (2021) 102 [arXiv:2006.11382] [INSPIRE].

[100] A. Gehrmann-De Ridder et al., *NNLO QCD corrections for Z boson plus jet production*, *PoS* **RADCOR2015** (2016) 075 [arXiv:1601.04569] [INSPIRE].

[101] E. Fox, N. Glover and M. Marcoli, *Generalised antenna functions for higher-order calculations*, *JHEP* **12** (2024) 225 [arXiv:2410.12904] [INSPIRE].

[102] F. Devoto et al., *Towards a general subtraction formula for NNLO QCD corrections to processes at hadron colliders: final states with quarks and gluons*, *JHEP* **08** (2025) 122 [arXiv:2503.15251] [INSPIRE].

[103] G. Bertolotti et al., *NNLO subtraction for any massless final state: a complete analytic expression*, *JHEP* **07** (2023) 140 [*Erratum ibid.* **05** (2024) 019] [arXiv:2212.11190] [INSPIRE].

[104] M.A. Ebert et al., *SCETlib: a C++ package for numerical calculations in QCD and soft-collinear effective theory*, DESY-17-099 (2018).

[105] G. Lustermans, J.K.L. Michel, F.J. Tackmann and W.J. Waalewijn, *Joint two-dimensional resummation in q_T and 0-jettiness at NNLL*, *JHEP* **03** (2019) 124 [arXiv:1901.03331] [INSPIRE].

[106] J.C. Collins and D.E. Soper, *Back-To-Back Jets in QCD*, *Nucl. Phys. B* **193** (1981) 381 [*Erratum ibid.* **213** (1983) 545] [INSPIRE].

[107] J.C. Collins and D.E. Soper, *Back-To-Back Jets: Fourier Transform from B to K-Transverse*, *Nucl. Phys. B* **197** (1982) 446 [INSPIRE].

[108] J.C. Collins, D.E. Soper and G.F. Sterman, *Transverse Momentum Distribution in Drell-Yan Pair and W and Z Boson Production*, *Nucl. Phys. B* **250** (1985) 199 [INSPIRE].

[109] T. Becher and M. Neubert, *Drell-Yan Production at Small q_T, Transverse Parton Distributions and the Collinear Anomaly*, *Eur. Phys. J. C* **71** (2011) 1665 [arXiv:1007.4005] [INSPIRE].

[110] S. Catani, D. de Florian and M. Grazzini, *Universality of nonleading logarithmic contributions in transverse momentum distributions*, *Nucl. Phys. B* **596** (2001) 299 [hep-ph/0008184] [INSPIRE].

[111] M.G. Echevarria, A. Idilbi and I. Scimemi, *Factorization Theorem For Drell-Yan At Low q_T And Transverse Momentum Distributions On-The-Light-Cone*, *JHEP* **07** (2012) 002 [arXiv:1111.4996] [INSPIRE].

[112] J.-Y. Chiu, A. Jain, D. Neill and I.Z. Rothstein, *A Formalism for the Systematic Treatment of Rapidity Logarithms in Quantum Field Theory*, *JHEP* **05** (2012) 084 [arXiv:1202.0814] [INSPIRE].

[113] J.C. Collins and T.C. Rogers, *Equality of Two Definitions for Transverse Momentum Dependent Parton Distribution Functions*, *Phys. Rev. D* **87** (2013) 034018 [arXiv:1210.2100] [INSPIRE].

[114] Y. Li, D. Neill and H.X. Zhu, *An exponential regulator for rapidity divergences*, *Nucl. Phys. B* **960** (2020) 115193 [arXiv:1604.00392] [INSPIRE].

JHEP01(2026)065

[115] M.A. Ebert et al., *Subleading power rapidity divergences and power corrections for q_T*, *JHEP* **04** (2019) 123 [arXiv:1812.08189] [INSPIRE].

[116] D. Baranowski et al., *Zero-Jettiness Soft Function to Third Order in Perturbative QCD*, *Phys. Rev. Lett.* **134** (2025) 191902 [arXiv:2409.11042] [INSPIRE].

[117] M.A. Ebert, B. Mistlberger and G. Vita, *N-jettiness beam functions at N^3LO*, *JHEP* **09** (2020) 143 [arXiv:2006.03056] [INSPIRE].

[118] R. Brüser, Z.L. Liu and M. Stahlhofen, *Three-Loop Quark Jet Function*, *Phys. Rev. Lett.* **121** (2018) 072003 [arXiv:1804.09722] [INSPIRE].

JHEP01(2026)065